Constraints on Field Galaxy Halos from Weak Lensing and Satellite Dynamics

Tereasa G. Brainerd

Boston University, Institute for Astrophysical Research, 725 Commonwealth Ave., Boston, MA 02215

Abstract. Here I summarize constraints on the nature of the dark matter halos of field galaxies that have been obtained from the most recent investigations of (i) weak galaxy–galaxy lensing and (ii) the dynamics of satellite galaxies in orbit about large host galaxies. Both of these techniques are statistical in their nature (i.e., large samples of galaxies are required to obtain a "signal"), but since they have inherently different selection biases and systematic errors, they are quite complementary to each other. Results of work over the last several years on weak lensing and satellite dynamics is revealing a remarkably consistent picture regarding the dark matter halos of bright field galaxies ($L \gtrsim L^*$). The halos extend to large physical radii ($\gtrsim 150\ h^{-1}$ kpc) and are flattened in projection on the sky, there is a marked difference in the depths of the potential wells of early–type galaxies and late–type galaxies, and the velocity dispersion profiles of the halos, $\sigma_v(r_p)$, decrease at large projected radii. All of these are expected to hold true in a cold dark matter universe and, while neither technique can address the possible small–scale ($\lesssim 5\ h^{-1}$ kpc) conflicts between cold dark matter and observed galaxies, on scales $\gtrsim 50\ h^{-1}$ kpc both techniques yield results that are consistent with each other, and with the predictions of cold dark matter.

INTRODUCTION

The existence of dark matter halos surrounding large, bright galaxies is well established (e.g., [1], [2], [3], [4] and references therein), and in the standard cold dark matter (CDM) paradigm, the halos of large field galaxies are expected to extend to virial radii of $\sim 100h^{-1}$ kpc to $\sim 200h^{-1}$ kpc and have masses of $\sim 10^{12}h^{-1}M_{\odot}$ (e.g., [5], [6], [7]). Until very recently, however, direct observational constraints on the nature of the dark matter halos of field galaxies have not been especially strong. In particular, it has been challenging to address the question as to whether the halos of observed galaxies are consistent with the halos that one would expect in a CDM universe.

The lack of a Keplerian fall–off in the rotation curves of the disks of most spiral galaxies (e.g., [2]) indicates that the dark matter halos extend far beyond the visible radii of the galaxies. Therefore, in order to place constraints on the total mass distribution, it is necessary to use tracers of the halo potential that exist at large projected radii ($\gtrsim 100h^{-1}$ kpc). Two such tracers of the large–scale potential are satellite galaxies that are in orbit about isolated host galaxies, and photons emitted by distant galaxies that, on their way to the observer, happen to pass through the potential wells of more nearby galaxies at small impact parameters (i.e., gravitational lensing). "Strong" gravitational lensing, in which multiple and highly–distorted images of a source occur, is a rare phenomenon because it requires nearly perfect alignment of the lens and source galaxy (e.g., [8]). "Weak" gravitational lensing, in which multiple images and significant image distortion do not occur, is, however, commonplace in the universe (e.g., [9], [10], [11], [12]), and it is on this extremely mild regime of gravitational lensing that I will focus for this discussion.

Weak lensing of background galaxies by foreground galaxies ("galaxy–galaxy" lensing) and the motions of satellite galaxies about host galaxies are phenomena that can only lead to constraints on halo potentials through ensemble averages over statistically large samples. That is, for any given foreground galaxy, the distortion that it induces in the images of background galaxies due to weak lensing is so small that the signal cannot be detected convincingly for any one foreground lens galaxy. Similarly, isolated host galaxies are typically found to have 1 to 2 satellite galaxies on average and, so, the potential of any one host galaxy cannot be constrained at all well by the motions of its own satellites. Both galaxy–galaxy lensing and satellite dynamics, therefore, lead to statistical constraints on the halo population as a whole and by their very nature they require large samples of galaxies in order to obtain such constraints. Until several years ago, galaxy–galaxy lensing and satellite dynamics were both tantalizingly close (or frustratingly close, depending on one's point of view) to being able to fulfill their theoretical promise to map out the gravitational potentials of the halos of field galaxies. With the advent of routine availability of wide–field imagers

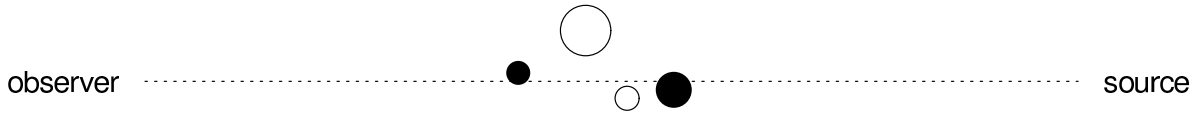

FIGURE 1. Schematic representation of multiple lenses along the line of sight to a given source galaxy.

and the completion (or near completion) of large redshift surveys, however, both galaxy–galaxy lensing and satellite dynamics are now yielding sufficiently strong constraints on the dark matter halos of galaxies that the observations can be used to test the theoretical predictions (i.e., CDM) at a substantive level.

There are distinct advantages and disadvantages of galaxy–galaxy lensing versus satellite dynamics when it comes to constraining halo potentials. A clear advantage of galaxy–galaxy lensing is that it can be applied to *all* foreground galaxies and, since gravitational lensing is affected only by the total mass along the line of sight and not its dynamical state, the halos of the foreground lens galaxies need not be virialized. A complicating factor in galaxy–galaxy lensing is that it is not correct to assume that each background galaxy has been lensed solely by one foreground galaxy (e.g., [13], [14], [15]). Instead, photons emitted by the distant galaxies are deflected by *all* mass along the line of sight, including individual galaxies, groups, and clusters (e.g., Figure 1). That is, galaxy–galaxy lensing is inherently a multiple–deflection problem and care must be taken when using observations of galaxy–galaxy lensing to constrain the halos of a given subset of lens galaxies (i.e., the halos of early–type galaxies versus late–type galaxies, or the halos of high–luminosity galaxies versus low–luminosity galaxies). Therefore, a computation of the weak lensing signal about the white lenses in Figure 1 above is *not* identical to a measurement of weak lensing signal *produced by* the white lenses since the black lenses also contribute to the net shape of the final image. That is not to say that galaxy–galaxy lensing cannot be used to probe the potentials of halos surrounding lenses of differing types; it most certainly can, but the presence of multiple deflections in the data must be taken into account when modeling the observed signal. In the case of relatively shallow data ($z_{\rm lens} \sim 0.15$), most sources will have been lensed by only one foreground galaxy (e.g., [16]), but in deep data sets ($z_{\rm lens} \sim 0.5$) most source galaxies will have been lensed at a significant and comparable level by two or more foreground galaxies (e.g., [13], [15]). A further disadvantage of galaxy–galaxy lensing is that the signal is very small (systematic image distortions of $\lesssim 1\%$ or in the image ellipticities), so the images of millions of background galaxies must be obtained and, in general, be meticulously corrected for the presence of anisotropic, spatially–varying point spread functions. Finally, it is possible that Newtonian tidal distortions of genuine satellites of the lens galaxies could masquerade as a weak lensing signal. Happily, such distortions appear to be at most a very small contributor to the observed weak lensing signal (e.g., [13], [17]. [18], [19]).

An advantage to using dynamics of satellite galaxies to probe the potentials of the halos of isolated host galaxies is that, unlike deep weak lensing data, the only important potential well in the problem is that of the host galaxy. In principle, this is a "cleaner", more straightforward probe of the halo potential which is intentionally restricted to the physical scales that one would expect to characterize the halos of individual large galaxies. However, there are a number of arguments against the use of satellite dynamics to probe the mass distributions of host galaxies: (1) satellites must be found at large projected radii in order to probe the halo potential on the very largest scales, (2) noise is introduced by the presence of "interlopers" (i.e., galaxies that are selected as satellites but which are, in fact, not associated dynamically with the host galaxy), and (3) the relaxation times of these systems are large compared to the age of the universe. The first argument is much less compelling now than it was in the past simply because of the availability of large redshift surveys (i.e., the data bases are now sufficiently big that although it is rare to find satellites at, say, a projected radius of 500 h^{-1} kpc, the large number of redshifts that are now available makes it possible to compile statistically significant samples). The second argument has also become much less compelling with the realization that it is straightforward to account for the effects of interloper galaxies on the determination of the velocity dispersion (see below). The third argument can still be compelling, since it makes little sense to apply a virial–type mass estimator to systems which are not relaxed. However, an assumption of virialization is not necessary *a priori*, and the use of secondary infall models can be used to bypass this assumption (e.g., [20]).

For the sake of a certain amount of brevity and, at the very least, an attempt at providing some level of coherent argument, I will focus here on only the most recent results that are directly relevant to the halos of field galaxies and which have been obtained from four large surveys: the COMBO–17 Survey, the Red–Sequence Cluster Survey (RCS),

the Sloan Digital Sky Survey (SDSS), and the Two Degree Field Galaxy Redshift Survey (2dFGRS). Even with this restriction, it is simply not possible to discuss all of the most recent results from these studies in great detail, and the reader should consult the source literature for further information. Finally, I should hasten to add that all errors or omissions in this article in regards to my colleagues' work are entirely unintentional and entirely my own fault. I can only hope that my colleagues will be kind enough to forgive me.

THE SURVEYS

COMBO–17: Galaxy–Galaxy Lensing

The acronym COMBO–17 stands for "Classifying Objects by Medium–Band Observations in 17 filters" [21], [22], [23]. The COMBO–17 survey consists of high–quality imaging data with the ability to obtain both rest frame colors and accurate photometric redshifts ($\delta z/(1+z) < 0.01$ for $R < 21$, $\delta z/(1+z) \sim 0.02$ for $R \sim 22$, and $\delta z_{\rm phot} < 0.1$ for $R < 24$). The survey consists of 5 fields, including an extended region in the location of the Chandra Deep Field South (CDFS). The observations were carried out using the Wide Field Imager at the 2.2–m MPG/ESO telescope. The field of view of the camera is $34' \times 33'$ and the 17–band filter set covers a wavelength range of 350 nm $\lesssim \lambda_{\rm obs} \lesssim$ 930 nm. The latter allows for a rough determination of the spectral energy distributions of the objects, which in turn leads to both reliable classification of the objects into galaxies, quasars, and stars, as well as the ability to determine accurate photometric redshifts. A catalog containing astrometry, photometry in all 17 bands, object classification, and photometric redshifts for the 63,501 objects in the extended CDFS is publicly–available [23] (see `http://cdsweb.u-strasbg.fr/cgi-bin/qcat?J/A+A/421/913`). The COMBO–17 results that will be discussed here consist of efforts to use galaxy–galaxy lensing to study dark matter halos. The data set is particularly well–suited to this task because of the reliability with which background galaxies (i.e., lensed sources) can be separated from foreground galaxies (i.e., the lenses). Note, too, that although the full COMBO–17 survey covers 5 fields, the results shown here come from only 3 of the fields (a field centered on the cluster A901, the CDFS field, and a random field [24]).

RCS: Galaxy–Galaxy Lensing

The RCS ([25], [26]) is a somewhat shallow (5σ point source detection limits of $R_C \sim 24.8$ and $z' \sim 23.6$), wide field ($\sim$ 90 sq. deg.) imaging survey that was designed primarily to search for galaxy clusters out to redshifts of $z \sim 1.4$. The images for the complete survey were obtained with the CFHT and CTIO 4–m telescopes using mosaic cameras, and consist of 22 widely–separated patches of $\sim 2.1^\circ \times 2.3^\circ$. The RCS results that will be discussed here consist of galaxy–galaxy lensing studies and were obtained from $\sim$ 42 sq. deg. of northern RCS data. Without spectroscopic or photometric redshift information, the RCS galaxy–galaxy results had to be obtained from a rough separation of lenses and sources that was based upon apparent magnitude cuts (i.e., galaxies with "faint" apparent magnitudes are on average background objects while galaxies with "bright" apparent magnitudes are on average foreground objects). Although the foreground–background distinction between a given pair of galaxies in the RCS data is by no means as secure as in the COMBO–17 data, the RCS is nevertheless a superb data set for galaxy–galaxy studies simply because of the area covered ($\sim$ 45 times larger than COMBO–17 for the weak lensing work). Given that weak lensing is primarily a statistical game, this is a good example of how well the galaxy–galaxy lensing signal can be detected and also used to constrain the nature of dark matter halos given only minimal distance information and a tremendous number of candidate lenses and sources.

SDSS: Galaxy–Galaxy Lensing & Satellite Dynamics

The SDSS is a combined photometric and spectroscopic survey that will ultimately map roughly one quarter of the sky above $l \sim 30^\circ$ and provide redshifts of $\sim 10^6$ galaxies and $\sim 10^5$ quasars with $r' \lesssim 17.8$. The SDSS is a fully–digital survey and makes use of 5 broad optical bands (u', g', r', i', z') for photometry. The data for the SDSS are being acquired at the Apache Point Observatory in Sunspot, New Mexico using a 2.5–m telescope, as well as three, smaller subsidiary telescopes for the purposes of photometric calibration, monitoring of the seeing, and scanning for clouds.

The rms galaxy redshift errors are $\sim$ 20 km sec^{-1}to $\sim$ 30 km sec^{-1}(e.g., [27], [28]). A technical summary of the SDSS can be found in York et al. [29], information about the main galaxy sample is given by Strauss et al. [30], and information about the photometric system and photometric calibration is given by Fukugita et al. [31], Hogg et al. [32], and Smith et al. [33]. All of the SDSS data, including astrometry, photometry, redshifts, and spectra, are available via the SDSS website (`http://www.sdss.org`) using structured queries that can search and combine the individual data bases. The third SDSS data release occurred on September 27, 2004 and includes spectra of 374,767 galaxies, spectra of 51,027 quasars, and photometry of 141 million unique objects. The SDSS results that will be discussed here consist of both galaxy–galaxy lensing studies and studies of the satellites of large, isolated galaxies.

2dFGRS: Satellite Dynamics

The 2dFGRS is a spectroscopic survey in which the target objects were selected in the b_J band from the Automated Plate Measuring (APM) galaxy survey ([34], [35]) and extensions to the original survey. A detailed discussion of the survey and the data base is given by Colless et al. [36]. The observations, which are now complete, were carried out at the Anglo–Australian Telescope using the Two Degree Field (2dF) multifiber spectrograph. The final data release occurred on June 30, 2003 [37] and includes reliable redshifts of 221,414 galaxies with extinction corrected magnitudes of $b_J \geq 19.45$, covering an area over $\sim$ 1500 square degrees. Galaxies with reliable redshifts have an rms uncertainty of 85 km sec^{-1}[36]. All data, including spectroscopic catalogs (245,591 objects), photometric catalogs (382,323 objects), and FITS files containing the spectra, are publicly–available from the 2dFGRS website (`http://msowww.anu.edu/au/2dFGRS`). The 2dFGRS data base is fully–searchable via structured queries, and on–line documentation is available on the 2dFGRS website. The photometric transformation from the SDSS band passes to b_J is

$$b_J = g' + 0.155 + 0.152(g' - r') \tag{1}$$

(e.g., [38]). The 2dFGRS results that will be discussed here consist of investigations into the nature of the dark matter halos of large, isolated galaxies that are orbited by one or more satellite galaxies.

PROBING HALO POTENTIALS WITH WEAK LENSING

General Relativity tells us that any mass will cause a curvature of spacetime in its vicinity. Therefore, any mass located along the line of sight to a distant luminous object will act as a gravitational lens by deflecting light rays emanating from the object as they propagate through the universe. The most striking instances of gravitational lensing (e.g., multiple images, rings, arcs) are examples of rare phenomena caused by strong gravitational lenses, which greatly distort the images of distant galaxies. In contrast to this, weak gravitational lenses distort the images of distant galaxies very little but produce a net coherent pattern of image distortions in which there is a slight preference for the lensed galaxies to be oriented tangentially with respect to the direction vector that connects their centroids with the center of the gravitational potential of the lens. While weak lenses do not give rise to stunning individual images, they are detectable in a statistical sense via ensemble averages over many mildly–distorted images (e.g., [9], [10], [11], [12]).

Provided the distance traveled by the light ray is very much greater than the scale size of the lens, it is valid to adopt the "thin lens approximation" in order to describe a gravitational lens. Consider a lens with an arbitrary 3-dimensional potential, Φ. In the thin lens approximation a conveniently scaled 2-dimensional potential for the lens (i.e., the 3-dimensional potential of the lens integrated along the optic axis) is given by

$$\psi(\vec{\theta}) = \frac{D_{ls}}{D_l D_s} \frac{2}{c^2} \int \Phi(D_d \vec{\theta}, z) dz, \tag{2}$$

where $\vec{\theta}$ is the location of the lensed image on the sky, measured with respect to the optic axis, and D_{ls}, D_l, and D_s are angular diameter distances between the lens and source, observer and lens, and observer and source, respectively (e.g., [8]). It is then straightforward to relate the gravitational potential of the lens to the two fundamental quantities that characterize the lens: the convergence (κ) and the shear ($\vec{\gamma}$). The convergence, which describes the isotropic focusing of light rays, is given by

$$\kappa(\theta) = \frac{1}{2} \left(\frac{\partial^2 \psi}{\partial \theta_1^2} + \frac{\partial^2 \psi}{\partial \theta_2^2} \right). \tag{3}$$

The shear describes tidal gravitational forces acting across a bundle of light rays and, therefore, the shear has both a magnitude, $\gamma = \sqrt{\gamma_1^2 + \gamma_2^2}$, and an orientation, φ. In terms of ψ, the components of the shear are given by

$$\gamma_1(\vec{\theta}) = \frac{1}{2}\left(\frac{\partial^2\psi}{\partial\theta_1^2} - \frac{\partial^2\psi}{\partial\theta_2^2}\right) \equiv \gamma(\vec{\theta})\cos\left[2\varphi(\theta)\right] \tag{4}$$

and

$$\gamma_2(\vec{\theta}) = \frac{\partial^2\psi}{\partial\theta_1\partial\theta_2} = \frac{\partial^2\psi}{\partial\theta_2\partial\theta_1} \equiv \gamma(\vec{\theta})\sin\left[2\varphi(\vec{\theta})\right]. \tag{5}$$

The effect of convergence and shear acting together in a gravitational lens is to distort the images of distant objects. Consider a source galaxy which is spherical in shape. In the absence of a gravitational lens, an observer would see an image of the galaxy which is truly circular. If a gravitational lens is interposed along the line of sight to the distant galaxy, the observer will see an image which, to first order, is elliptical and the major axis of the ellipse will be oriented tangentially with respect to the direction vector on the sky that connects the centroids of the image and the lens. That is, the circular source is distorted into an ellipse, and to first order the distortion consists of both a tangential stretch of $(1-\kappa-\gamma)^{-1}$ and a radial compression of $(1-\kappa+\gamma)^{-1}$ (e.g., [8]). In the weak lensing regime, both the convergence and shear are small ($\kappa << 1$ and $\gamma << 1$).

The fundamental premise in all attempts to detect weak lensing is that, in the absence of lensing, galaxy images have an intrinsically random ellipticity distribution. Gravitational lensing then introduces a shift in the ellipticity distribution that, in the mean, manifests as a tangential alignment of background sources around foreground lenses. The image of a distant galaxy can be approximated an ellipse with complex image ellipticity given by

$$\varepsilon = \frac{a^2-b^2}{a^2+b^2}e^{2i\phi} = \varepsilon_1 + i\varepsilon_2, \tag{6}$$

where a and b are the major and minor axes, respectively, and ϕ is the position angle. The complex image ellipticity is often referred to as the "image polarization" (e.g., [39]) and is computed in terms of flux–weighted second moments,

$$Q_{i,j} = \sum_{i,j} I_{i,j} W_{i,j} x_i x_j, \tag{7}$$

where $I_{i,j}$ is the intensity at a given pixel and $W_{i,j}$ is a weighting function. The real and imaginary components of the image polarization are then given by:

$$\varepsilon_1 = \frac{Q_{1,1}-Q_{2,2}}{Q_{1,1}+Q_{2,2}}, \qquad \varepsilon_2 = \frac{2Q_{1,2}}{Q_{1,1}+Q_{2,2}}. \tag{8}$$

The *observed* image polarization for any one source is, of course, a combination of its intrinsic ellipticity and any ellipticity that is induced by lensing. In the limit of weak lensing, the observed image polarization, $\varepsilon^{\rm obs}$, is related to the intrinsic image polarization, $\varepsilon^{\rm int}$ through a shift in the complex plane. Although we cannot determine $\varepsilon^{\rm int}$ for any one particular source galaxy, we have that the mean intrinsic ellipticity distribution for an ensemble of source galaxies is $\left\langle\varepsilon^{\rm int}\right\rangle = 0$ since the galaxies should be randomly–oriented in the absence of lensing. An estimator for the shear induced by weak lensing is then $\gamma = \left\langle\varepsilon^{\rm obs}\right\rangle/2$ (e.g., [39]). This simple estimator does not reflect the fact that the way in which the shear alters the shape of a source depends upon its intrinsic ellipticity, and in practice this is generally taken into account when computing the shear. See, e.g., [40], [41], and [42] for discussions of the "shear polarizability" and "shear responsivity" of sources. In addition, it is worth noting that, while it is common practice to approximate image shapes as ellipses, there will be some images that have been sufficiently distorted by galaxy–galaxy lensing that a mild bending, or "flexion", of the images will occur and such images cannot be accurately represented as ellipses. In principle, flexion of images can be used to detect weak lensing with a signal–to–noise that is increased over the common practice of fitting equivalent image ellipses [43], [44]. A preliminary application of this technique [43] has been carried out with the Deep Lens Survey [45], and it will be interesting to see how the technique is further developed and implemented in practice.

The first attempts to detect systematic weak lensing of background galaxies by foreground galaxies ([46], [47]) were met with a certain degree of skepticism because the apparent distortion of the source galaxy images was rather smaller than one would expect based upon the typical rotation velocities of the disks of large spiral galaxies. The situation

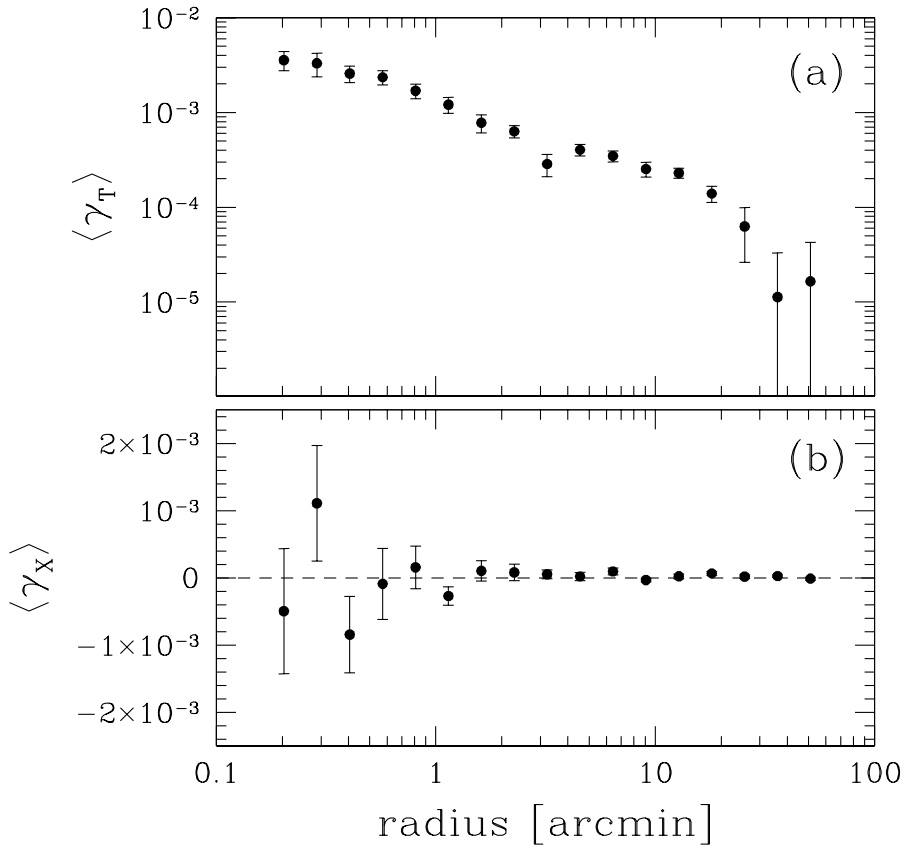

FIGURE 2. a) Mean tangential shear computed about the lens centers in ~ 42 sq. deg. of the RCS [48]. Here foreground galaxies and background galaxies have been separated on the basis of apparent magnitude alone. Bright, lens galaxies have $19.5 < R_C < 21$ and faint, source galaxies have $21.5 < R_C < 24$. b) Same as in a) except that here each background galaxy image has been rotated by 45°. This is a control statistic and in the absence of systematic errors it should be consistent with zero on all scales. Figure kindly provided by Henk Hoekstra.

changed when Brainerd, Blandford & Smail [13] measured the orientations of 506 faint galaxies ($23 < r_f \leq 24$) with respect to the locations of 439 bright galaxies ($20 \leq r_b \leq 23$) and found that the orientation of the faint galaxies was inconsistent with a random distribution at the 99.9% confidence level. The faint galaxies showed a clear preference for tangential alignment with the direction vector on the sky that connected the centroids of the faint and bright galaxies, in agreement with the expectations of systematic weak lensing of the faint galaxies by the bright galaxies.

Almost immediately, a number of similar investigations followed in the wake of Brainerd, Blandford & Smail [13] ([49], [50], [51], [52], [53], [54], [55]). These studies made use of a wide variety of data and analysis techniques, and all were broadly consistent with one another and with the results of Brainerd, Blandford & Smail [13] (see, e.g., the review by Brainerd & Blandford [14]). The first truly undeniable detection of galaxy–galaxy lensing was obtained by Fischer et al. [53] with 225 sq. deg. of early commissioning data from the SDSS, and it was this result in particular that helped to make the study of galaxy–galaxy lensing into a respectable endeavor, whereas previously many had considered the whole field rather dodgy at best. Fisher et al. [53] demonstrated conclusively that even in the limit of somewhat poor imaging quality, including the presence of an anisotropic point spread function due to drift scanning, galaxy–galaxy lensing can be detected with very high significance in wide–field imaging surveys. In the last few years, detections of galaxy–galaxy lensing and the use of the signal to constrain the dark matter halos of field galaxies has improved dramatically ([24], [42], [48], [56], [57], [58], [59], [60], [61]) owing to a number of factors that include such things as very large survey areas, sophisticated methods for correcting image shapes due to anisotropic and spatially–varying point spread functions, and the use of distance information for large numbers foreground lens galaxies in the

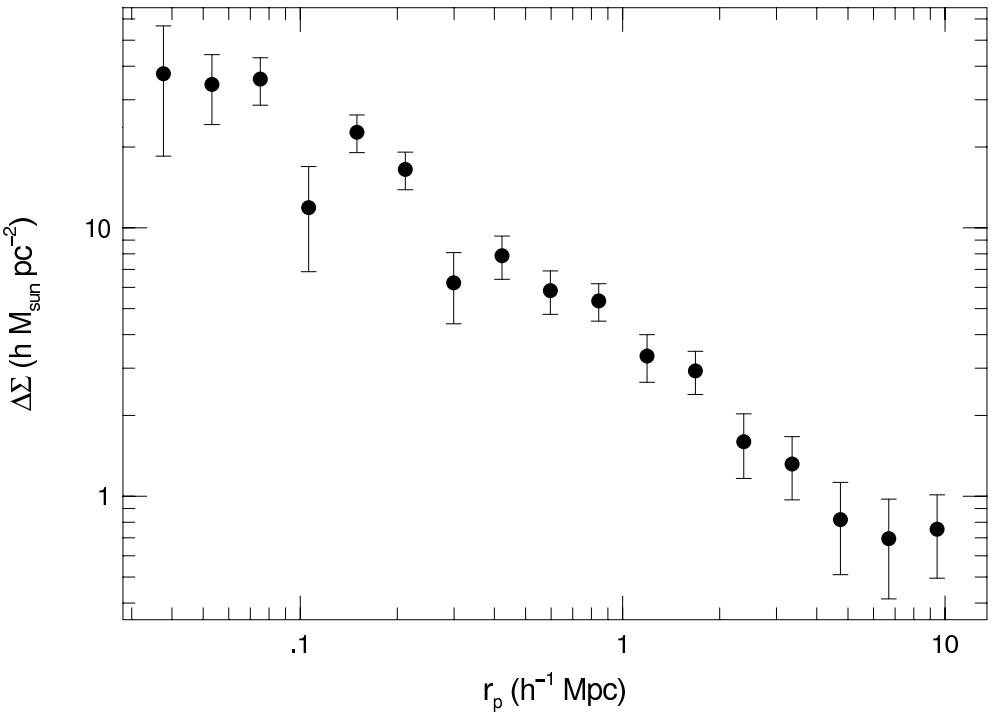

FIGURE 3. Mean excess projected mass density around weak galaxy lenses in the SDSS [42]. Here $\sim 1.27 \times 10^5$ lenses with spectroscopic redshifts and $\sim 9.0 \times 10^9$ sources with photometric redshifts have been used in the calculation. The values of $\Delta\Sigma(r_p)$ shown in this figure have been corrected for the clustering of the sources around the lenses. Data kindly provided by Erin Sheldon.

form of either spectroscopic or photometric redshifts.

Figure 2 shows one example of the high statistical significance with which weak lensing due to galaxies is now being routinely detected. The result comes from an analysis of the distortion of the images of $\sim 1.5 \times 10^6$ source galaxies due to $\sim 1.2 \times 10^5$ lens galaxies in the RCS [48], where the lens and source populations were separated solely on the basis of their apparent magnitudes. The top panel of Figure 2 shows the mean tangential shear *computed* about the lens centers which, because of the clustering of the lens galaxies, is not simply interpreted as the tangential shear *due to* individual lens centers. Instead, it is a projected (i.e., 2–dimensional) galaxy–mass cross–correlation function, and in order to compute the average properties of the halos of the lens galaxies it is necessary to, e.g., make use of Monte Carlo simulations that include all of the multiple weak deflections that the sources have undergone. The bottom panel of Figure 2 shows a control statistic in which the tangential shear about the lens centers is computed after rotating the images of the sources by 45°. If the signal in the top panel of Figure 2 is caused by gravitational lensing, the control statistic in the bottom panel of Figure 2 should be consistent with zero (and indeed it is). Note that, although the tangential shear about the RCS lenses persists to scales of order 0.5°, the shear on such large scales is not indicative of the masses of individual lens galaxies; rather it reflects the intrinsic clustering of the lenses. It is also worth noting that less than decade ago observers were struggling to measure a tangential shear of $\lesssim 0.01$ with a modest degree of confidence. Now, however, confident detection of tangential shears of $\lesssim 0.0001$ is effectively "routine" in these extremely large data sets.

The mean tangential shear, $\gamma_T(r_p)$, in an annulus of projected radius r_p is related to the projected surface mass density of the lens through

$$\Sigma_c \gamma_T(r_p) = \overline{\Sigma}(r < r_p) - \overline{\Sigma}(r_p) \equiv \Delta\Sigma(r_p), \tag{9}$$

where $\overline{\Sigma}(r < r_p)$ is the mean surface mass density interior to the projected radius r_p, $\overline{\Sigma}(r_p)$ is the projected surface mass density at radius r_p (e.g., [62], [63], [58]), and Σ_c is the so–called critical surface mass density:

$$\Sigma_c \equiv \frac{c^2 D_s}{4\pi G D_l D_{ls}}, \tag{10}$$

where c is the velocity of light and D_s, D_l, and D_{ls} are again angular diameter distances [8]. The quantity $\Delta\Sigma(r_p)$ above is, therefore, a mean excess projected mass density. Shown in Figure 3 is the mean excess projected surface mass density in physical units of $h\ M_\odot\ \mathrm{pc}^{-2}$ for $\sim 1.27 \times 10^5$ lens galaxies in the SDSS for which spectroscopic redshifts are known [42]. In addition to spectroscopic redshifts for the lenses, photometric redshifts were used for $\sim 9.0 \times 10^9$ source galaxies. Moreover, because the redshifts of the lens galaxies are known, $\Delta\Sigma(r_p)$ can be computed as a function of the physical projected radius at the redshift of the lens (rather than an angular scale). In Figure 3, $\Delta\Sigma(r_p)$ has been corrected for the clustering of the sources around the lenses via a function which is effectively a weighted cross–correlation function between the lenses and sources [42].

Having obtained a measurement of $\gamma_T(\theta)$, or equivalently $\Delta\Sigma(r_p)$, constraints can then be placed on the nature of the dark matter halos of the lens galaxies by modeling the observed signal. As mentioned earlier, quite a bit of care has to be taken in doing this if the goal is to constrain the halo parameters as a function of, say, the host luminosity, color, or morphology (see, e.g., [16]). In the past few years, however, good constraints on the mass of an "average" halo associated with an L^* galaxy, as well as fundamental differences between the halos of L^* ellipticals versus L^* spirals, have emerged from galaxy–galaxy lensing studies and it is those studies which are summarized below.

PROBING HALO POTENTIALS WITH SATELLITE GALAXIES

In order to use satellite galaxies to probe the potentials of host galaxies, one needs to *define* an appropriate sample of host and satellite galaxies. Unlike cosmology simulators who are blessed with full 6-dimensional phase space information, observers are, of course, limited to 3 dimensions (RA, DEC, and redshift). Given this limited information, then, one must base the selection criteria on projected radii (evaluated at the redshift of the host) and relative radial velocities, dv, of the candidate hosts and satellites. To guarantee that the dynamics of the satellites are determined solely by their host galaxy, the hosts must be determined to be "isolated" in some sense. That is, if another large, bright galaxy is too close to a candidate host galaxy to guarantee that the satellite orbits are affected solely by the candidate host, that candidate host and its satellites are rejected from the sample. Satellites must, necessarily, be fainter than their host, be found within some reasonable projected radius of the host, and have some reasonable line of sight velocity with respect to the host.

There are a number of different selection criteria that have been used in the recent literature, and three sets of selection criteria that have been used in more than one investigation are summarized below:

1. Hosts must be at least 8 times brighter than any other galaxy that is within $r_p < 500$ kpc and $|dv| < 1000$ km sec^{-1}. In addition, hosts must be at least 2 times brighter than any other galaxy that is within $r_p < 1$ Mpc and $|dv| < 1000$ km sec^{-1}. Satellites must be at least 8 times fainter than their host, must be found within $r_p < 500$ kpc, and must have $|dv| < 500$ km sec^{-1}. Here $h = 0.7$ has been adopted ([20], [64]).
2. Hosts must be at least 2 times brighter than any other galaxy that falls within $r_p < 2.86$ Mpc and $|dv| < 1000$ km s^{-1}. Satellites must be at least 4 times fainter than their host, must be found within $r_p < 714$ kpc and must have $|dv| < 1000$ km s^{-1}. Here $h = 0.7$ has been adopted ([64], [65], [66], [67]).
3. Hosts must be at least 2.5 times brighter than any other galaxy that is within a projected radius of $r_p < 700$ kpc and a relative radial velocity difference of $|dv| < 1000$ km sec^{-1}. Satellites must be at least 6.25 times fainter than their host, must be found within $r_p < 500$ kpc, and the host–satellite velocity difference must be $|dv| < 500$ km sec^{-1}. Here $h = 0.7$ has been adopted ([64], [68]).

Although the above criteria may seem lax or even somewhat arbitrary, in the case of the first two sets of criteria, both the Milky Way and M31 would be excluded from the sample of hosts. That is, these particular selection criteria give rise to samples of unusually isolated host galaxies. In addition, both Prada et al. [27] and Brainerd [64] adopted a number of different selection criteria in their investigations of the satellites of SDSS galaxies and concluded that there were no statistical differences between results that were obtained with different selection criteria. In other words, provided sufficiently "reasonable" criteria are adopted for selecting isolated hosts and their satellites, the results of the investigations are stable to modest differences in the details of those selection criteria.

No matter what selection criteria are adopted, however, there will always be "interlopers" in the satellite data. Interlopers are galaxies that are falsely identified as satellites; that is, they pass the formal selection criteria, but they are not, in fact, dynamically associated with the host galaxy. The presence of interlopers will artificially inflate any measurement of the velocity dispersion of genuine satellites, and recent investigations of satellite dynamics ([27], [65], [66], [67]) have corrected for the effects of interlopers by modeling the distribution of host–satellite velocity

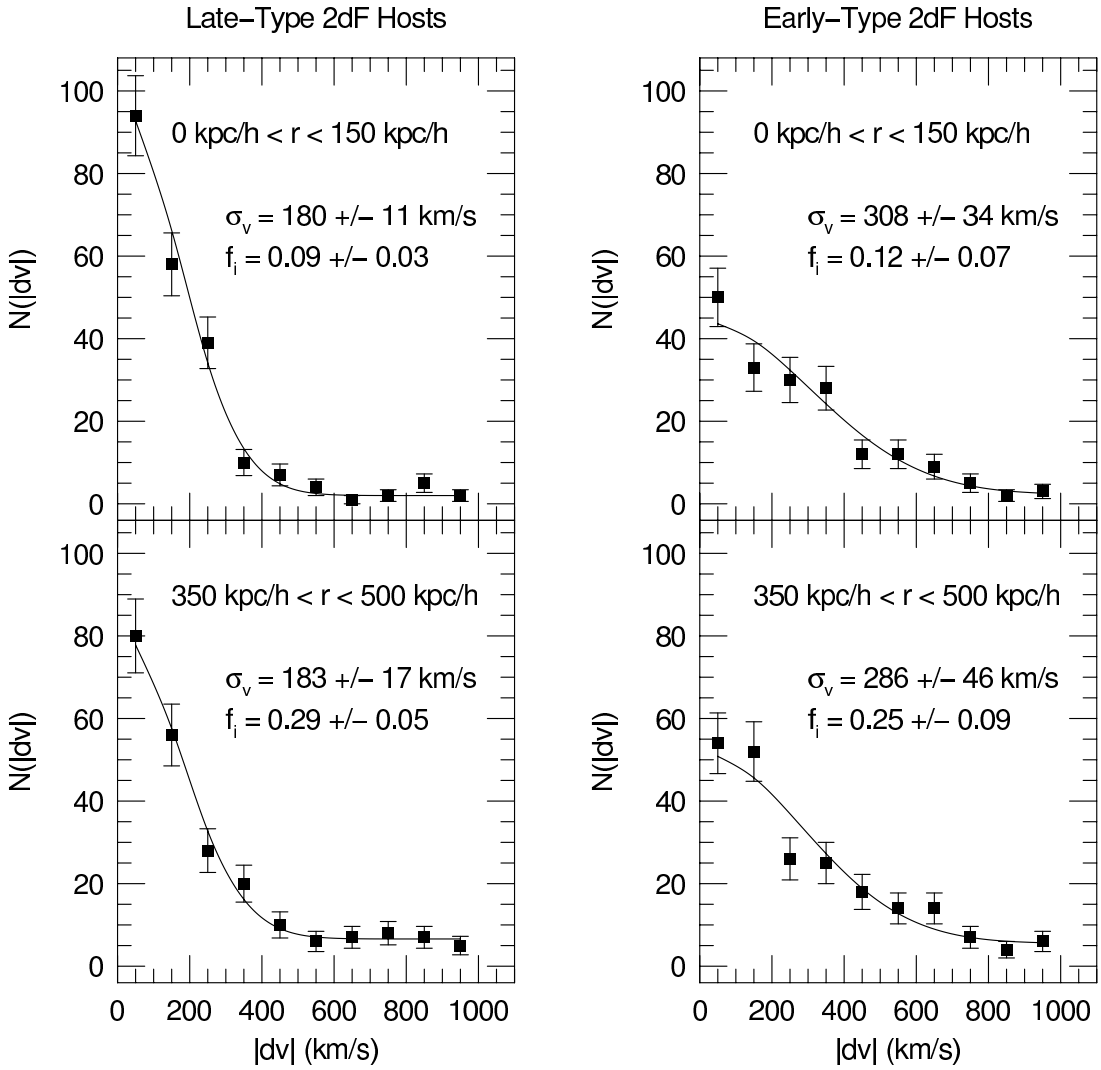

FIGURE 4. Points with error bars show the observed distribution of velocity differences, $N(|dv|)$, for a subset of host–satellite systems in the 2dFGRS for which the host morphologies have been visually classified. Solid lines show the best–fitting "Gaussian plus offset" function, from which the velocity dispersion of the satellites, σ_v, and the fraction of interlopers, f_i, is determined. Left panels: late–type hosts. Right panels: early–type hosts. Top panels: satellites located close to the host in projection on the sky. Bottom panels: satellites located far from the host in projection on the sky. A substantially larger value of σ_v is obtained for the satellites of early–type hosts than for the satellites of late–type hosts. Note, too, that the fraction of interlopers increases significantly with the projected radius, r, of the satellites.

differences as the sum of a Gaussian distribution (due to the genuine satellites) and a constant offset (due to the interlopers). Prada et al. [27] used numerical simulations to show that this is a sensible way in which to correct for the effects of interlopers. Moreover, both Brainerd & Specian [66] and Prada et al. [27] have pointed out that an accurate determination of the velocity dispersion profile, $\sigma_v(r_p)$, for satellite galaxies depends on a proper determination of the interloper fraction as an explicit function of the projected radius. That is, by purely geometrical effects, the interloper fraction is necessarily an increasing function of r_p. An example of fitting a "Gaussian plus offset" to the distribution of velocity differences for late–type galaxies and early–type galaxies in the 2dFGRS is shown in Figure 4. One can clearly see from this figure that the velocity dispersion of the satellites is a function of the morphology of the host galaxy (being larger for early–type hosts than late–type hosts), and that the interloper fraction increases with projected radius.

The above "Gaussian plus offset" fit to the distribution of host–satellite velocity differences accounts for the fact

that the number of interlopers is a function of projected radius, and it assumes *a priori* that the number of interlopers at a given projected radius is constant with $|dv|$. Recently, however, van den Bosch et al. [69] used simulations of galaxy redshift surveys to investigate this and found a sharp increase in the number of interlopers for small relative velocities. van den Bosch et al. [69] note, however, that the value of σ_v that is determined from a simple "Gaussian plus offset" fit is not strongly affected by the fact that the number of interlopers varies with $|dv|$. This is because the best–fitting value of σ_v is rather insensitive to the precise value of the interloper fraction. Brainerd [67] also finds that the number of interlopers is larger for small values of $|dv|$ than it is for large values of $|dv|$, but that the effect is not nearly as pronounced as found by van den Bosch et al. [69]. Given the size of the error bars on the distribution of host–satellite velocity differences in the current observational samples, then, it would appear that the simple "Gaussian plus offset" fit to the distribution of velocity differences is more than adequate to the task of estimating $\sigma_v(r_p)$.

THEORY: "UNIVERSAL" (NFW) HALOS VS. ISOTHERMAL HALOS

High–resolution CDM simulations have established the existence of a "universal" density profile for dark matter halos which results from generic dissipationless collapse (e.g., [5], [6], [7], [70], [71], [72], [73], [74], [75]). This density profile fits objects that span roughly 9 orders of magnitude in mass (ranging from the masses of globular star clusters to the masses of large galaxy clusters) and applies to physical scales that are less than the "virial" radius, r_{200}. Conventionally, r_{200} is defined to be the radius at which the spherically–averaged mass density reaches 200 times the critical mass density (e.g., [5], [6], [7]).

Navarro, Frenk & White [5], [6], [7] showed that the universal density profile for dark matter halos was fitted well by a function of the form

$$\rho(r) = \frac{\delta_c \rho_c}{(r/r_s)\,(1+r/r_s)^2}, \tag{11}$$

and halos having such a density profile are generally referred to as "NFW" halos. Here $\rho_c = \frac{3H^2(z)}{8\pi G}$ is the critical density of the universe at the redshift, z, of the halo, $H(z)$ is Hubble's parameter at that same redshift, and G is Newton's constant. The scale radius $r_s \equiv r_{200}/c$ is a characteristic radius at which the density profile agrees with the isothermal profile (i.e., $\rho(r) \propto r^{-2}$), c here is a dimensionless number known as the concentration parameter, and

$$\delta_c = \frac{200}{3}\frac{c^3}{\ln(1+c) - c/(1+c)} \tag{12}$$

is a characteristic overdensity for the halo.

Formally, the above fitting function for the radial density profiles of CDM halos converges to a steep, cuspy profile: $\rho(r) \propto r^{-1}$. The NFW fitting formula, however, was never intended to be extrapolated to very small radii (i.e., radii smaller than the practical resolution limits of the simulations) and much fuss has been made over whether observed galaxies actually show such cuspy inner density profiles (e.g., [76], [77], [78], [79], [80], [81], [82], [83]). More recent numerical work has shown that the density profiles of CDM halos do not, in fact, converge to a well–defined asymptotic inner slope (e.g., [84], [85] [86], [87]), and it has become increasingly clear that fair and direct comparisons of simulated galaxies with observed galaxies on very small physical scales is an extremely challenging thing to do (e.g., [88], [89]).

Weak lensing and satellite dynamics do not have the ability to provide any information whatsoever on the cuspiness (or lack thereof) in the central regions of galaxies. Instead, both are governed by the large–scale properties of the halos (i.e., the regime in which the NFW profile is known to be an excellent description of the density profiles of CDM halos) and, at least in principle, both have the potential to discriminate between NFW halos and simpler singular isothermal sphere halos.

The radial density profile of a singular isothermal sphere halo is given by

$$\rho(r) = \frac{\sigma_v^2}{2\pi G r^2} \tag{13}$$

(e.g., [90]), where σ_v is the velocity dispersion. The isothermal sphere is characterized by the single parameter σ_v, which is constant as a function of radius. A key prediction for NFW halos, however, is that the radial velocity dispersion will have a strong dependence upon the radius and this, of course, is inconsistent with the constant value of

the velocity dispersion that characterizes singular isothermal spheres. Specifically, on sufficiently small scales $\sigma_r(r)$ should *increase* with radius, and on large scales $\sigma_r(r)$ should *decrease* with radius. Hoeft, Mücket & Gottlöber [91] have shown that the radial velocity dispersion of NFW halos can be fitted by a function of the gravitational potential, $\Phi(r)$, of the form:

$$\sigma_r(r) = \left[a \left(\Phi_{\rm out} - \Phi(r) \right) \left(\frac{\Phi(r)}{\Phi_{\rm out}} \right)^{\kappa} \right]^{1/2}. \tag{14}$$

Note that $\sigma_r(r)$ above is not the "line of sight" velocity dispersion, since r is a true 3–dimensional radius in eqn. (14). The parameters a and κ have values of $a = 0.29 \pm 0.04$ and $\kappa = 0.41 \pm 0.03$, and $\Phi_{\rm out}$ is the outer potential of the halo. Therefore, we expect the dynamics within an NFW halo to differ fundamentally from the dynamics within an isothermal sphere halo.

In the case of weak lensing, NFW halos give rise to a distortion in the images of distant galaxies that differs somewhat from the distortion that would be yielded by an isothermal sphere halo (e.g., [92], [93]). The radial dependence of the shear for the isothermal sphere is given by:

$$\gamma_{\rm sis}(r_p) = \frac{2\pi}{r_p} \left(\frac{\sigma_v}{c} \right)^2 \frac{D_{ls} D_l}{D_s} \tag{15}$$

(e.g., [8]). Here c is the velocity of light and D_s, D_l, and D_{ls} are again angular diameter distances. In the case of NFW halos, the radial dependence of the shear is given by:

$$\gamma_{\rm nfw}(x) = \begin{cases} \frac{r_s \delta_c \rho_c}{\Sigma_c} g_<(x) & (x < 1) \\ \frac{r_s \delta_c \rho_c}{\Sigma_c} \left[\frac{10}{3} + 4 \ln\left(\frac{1}{2}\right) \right] & (x = 1) \\ \frac{r_s \delta_c \rho_c}{\Sigma_c} g_>(x) & (x > 1) \end{cases} \tag{16}$$

where $x \equiv r_p / r_s$, Σ_c is the critical mass density for gravitational lensing given by eqn. (10), and the functions $g_{<,>}(x)$ are explicitly independent of the cosmology:

$$g_<(x) = \frac{8 {\rm arctanh} \sqrt{\frac{1-x}{1+x}}}{x^2 \sqrt{1-x^2}} + \frac{4}{x^2} \ln\left(\frac{x}{2}\right) - \frac{2}{(x^2-1)} + \frac{4 {\rm arctanh} \sqrt{\frac{1-x}{1+x}}}{(x^2-1)(1-x^2)^{1/2}} \tag{17}$$

$$g_>(x) = \frac{8 \arctan \sqrt{\frac{x-1}{1+x}}}{x^2 \sqrt{x^2-1}} + \frac{4}{x^2} \ln\left(\frac{x}{2}\right) - \frac{2}{(x^2-1)} + \frac{4 \arctan \sqrt{\frac{x-1}{1+x}}}{(x^2-1)^{3/2}}. \tag{18}$$

(e.g., [92], [93]).

In the following sections I summarize the most recent attempts to study the dark matter halos of field galaxies through satellite dynamics and weak lensing, including attempts to distinguish between isothermal and NFW potentials on the basis of the velocity dispersion profile and on the weak lensing shear.

OBSERVED VELOCITY DISPERSION PROFILES

At best, galaxy–galaxy lensing and satellite dynamics have the potential to constrain the dependence of the line of sight velocity dispersion on the projected radius, $\sigma_v(r_p)$. Determining $\sigma_v(r_p)$ has proven to be quite a challenge to galaxy–galaxy lensing studies, in large part because the shear profiles of NFW lenses and isothermal sphere lenses are not dramatically different, except on the very smallest ($r < r_s$) and very largest ($r > r_{\rm vir}$) scales [93]. To date, only one tentative measurement of $\sigma_v(r_p)$ has been made from observations of galaxy–galaxy lensing [24]. Kleinheinrich et al. [24] modeled the lens galaxies in the COMBO–17 survey as singular isothermal spheres with velocity dispersions that scaled with luminosity as

$$\frac{\sigma_v}{\sigma_v^*} = \left(\frac{L}{L^*} \right)^{\eta} \tag{19}$$

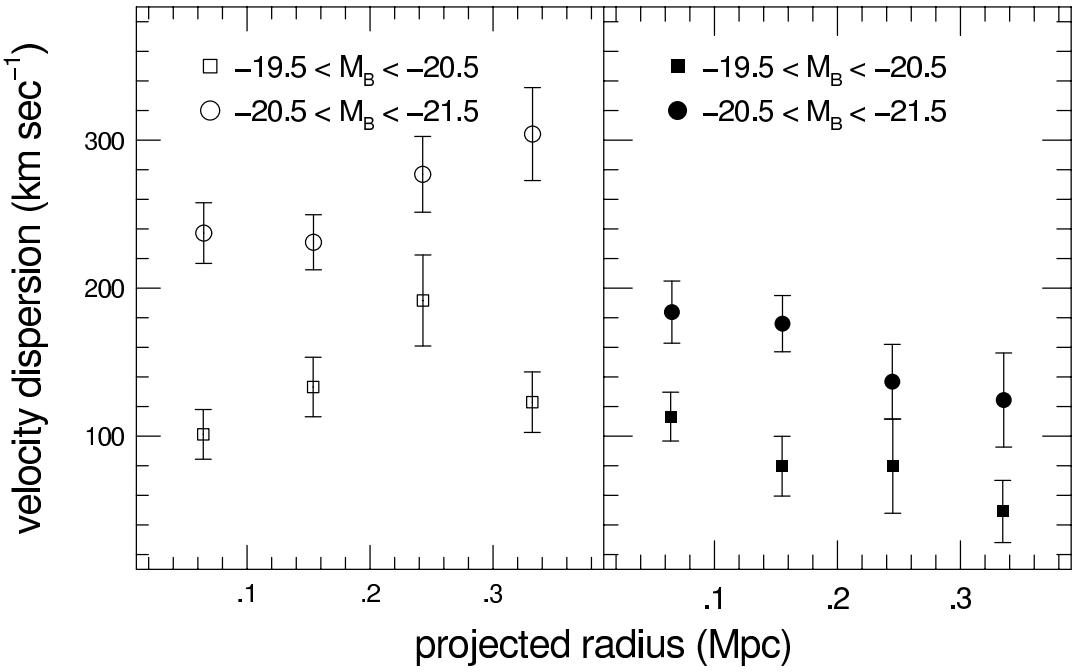

FIGURE 5. Velocity dispersion profiles for satellites of SDSS host galaxies [27]. Circles: host galaxies with $-20.5 < M_B < -21.5$, Squares: host galaxies with $-19.5 < M_B < -20.5$. Left panel: "raw" velocity dispersion profiles prior to correction for contamination by interlopers. Right panel: velocity dispersion profiles after correction for contamination by interlopers. After correction for interlopers, $\sigma_v(r_p)$ for the satellites of the fainter hosts is consistent with the expectations for an NFW halo with $M_{200} = 1.5 \times 10^{12} M_\odot$, and $\sigma_v(r_p)$ for the satellites of the brighter hosts is consistent with the expectations for an NFW halo with $M_{200} = 6 \times 10^{12} M_\odot$. Here $h = 0.7$ has been adopted.

where σ_v^* is the line of sight velocity dispersion of the halo of an L^* galaxy. Kleinheinrich et al. [24] fixed η to be 0.35 and determined best-fitting values of σ_v^* for projected radii in the range 20 h^{-1} kpc $< r_p < r_{\rm max}$. When they considered all lenses in their sample, Kleinheinrich et al. [24] found $\sigma_v^* \sim 139$ km sec^{-1}for $r_{\rm max} = 50$ h^{-1} kpc, $\sigma_v^* \sim 164$ km sec^{-1}for $r_{\rm max} = 150$ h^{-1} kpc, and $\sigma_v^* \sim 123$ km sec^{-1}for $r_{\rm max} = 500$ h^{-1} kpc. This suggests a velocity dispersion profile that rises at small radii, reaches a maximum, then decreases at large radii. However, the formal error bars on these measurements show that all of these values of σ_v^* agree to within one to two standard deviations. In addition, it should be kept in mind that each of these measurements of σ_v^* is not independent (as they would be if a differential measurement of $\sigma_v^*(r_p)$ were made), so the data points and their error bars are all correlated with one another.

Considerably stronger constraints on the dependence of the halo velocity dispersion with projected radius have come from the most recent investigations of the motions of satellites about host galaxies. In particular, both Prada et al. [27] and Brainerd [67] have measured decreasing velocity dispersion profiles for the satellites of host galaxies in the SDSS and 2dFGRS, respectively. Although they used different data sets and different host–satellite selection criteria, both Prada et al. [27] and Brainerd [67] used the same technique to make measurements of the velocity dispersion profiles. That is, the distribution of velocity differences, $N(|dv|)$, for satellites found within projected radii of $r_{\rm min} < r_p < r_{\rm max}$ was modeled as a combination of a Gaussian and an offset due to interlopers. In both studies, the interloper fraction was determined separately for each of the independent radial bins.

Prior to correcting for the contamination of interlopers, Prada et al. [27] found a velocity dispersion profile, $\sigma_v(r_p)$, that increased with projected radius. After the removal of the interlopers, however, Prada et al. [27] found decreasing velocity dispersion profiles in both cases. The corresponding velocity dispersion profiles are shown in Figure 5. Moreover, their corrected velocity dispersion profiles were fitted well by the velocity dispersion profiles of NFW halos with virial masses of 1.5×10^{12} $M_\odot$ (hosts with absolute magnitudes $-19.5 < M_B < -20.5$) and 6×10^{12} $M_\odot$

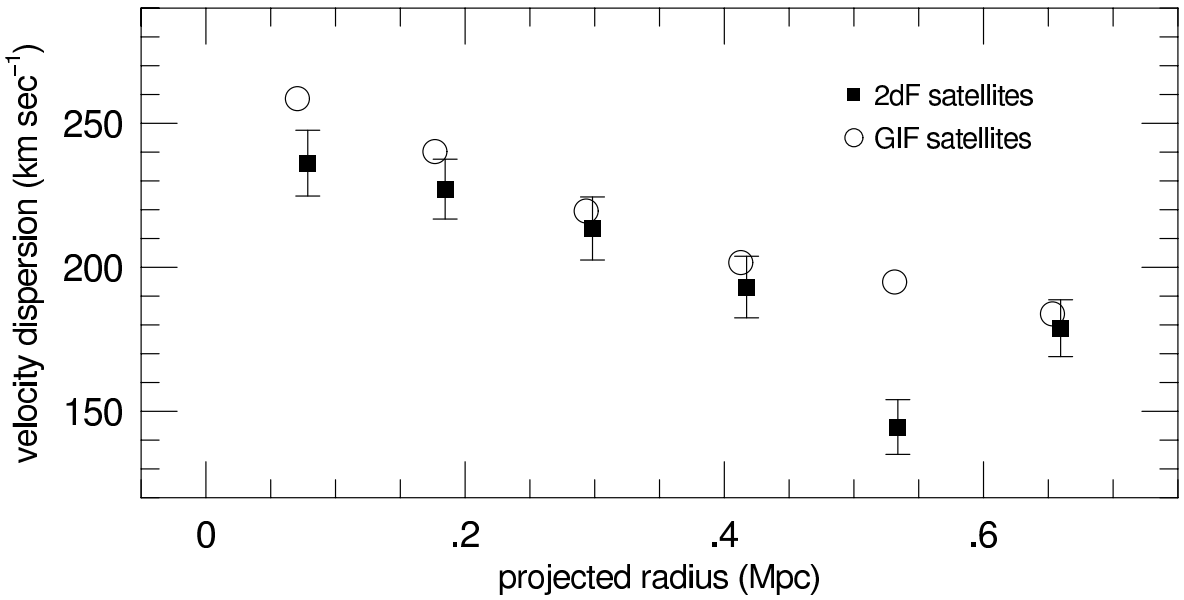

FIGURE 6. Velocity dispersion profiles for satellites in the final data release of the 2dFGRS and the flat, Λ–dominated GIF simulation [67]. Here $h = 0.7$ has been adopted.

(hosts with absolute magnitudes $-20.5 < M_B < -21.5$). Since Prada et al. [27] adopted a value of $h = 0.7$ and since the absolute magnitude of an L^* galaxy is $M_B^* \sim -19.5$, these results suggest that the virial mass of the halo of an L^* galaxy is $\lesssim 10 \times 10^{11} h^{-1} M_\odot$.

Brainerd [67] selected hosts and satellites from the final data release of the 2dFGRS using criteria identical to those of Sample 3 in Prada et al. [27]. In addition, she used these same criteria to select hosts and satellites from the present epoch galaxy catalogs of the flat, Λ–dominated the GIF simulation [94]. This is a publicly–available simulation which includes semi–analytic galaxy formation in a CDM universe. Brainerd [67] restricted her analysis to hosts with luminosities in the range $0.5\ L^* \leq L \leq 5.5\ L^*$, and found a roughly similar number of hosts and satellites in both the 2dFGRS (1345 hosts, 2475 satellites) and the GIF simulation (~ 1200 hosts, ~ 4100 satellites, depending upon the viewing angle). Like Prada et al. [27], Brainerd [67] obtained a decreasing velocity dispersion profile for the satellites of the 2dFGRS galaxies once the effects of interlopers were removed. In addition, excellent agreement between $\sigma_v(r_p)$ for the 2dFGRS galaxies and $\sigma_v(r_p)$ for the GIF galaxies was found, showing consistency between the motions of satellites in the 2dFGRS and the expectations of a Λ–dominated CDM universe. See Figure 6.

Further, Brainerd [67] divided her sample of 2dFGRS host galaxies into thirds based upon the spectral index parameter, η [95], and computed the dependence of the velocity dispersion profile on host spectral type. The subsamples corresponded to hosts which are expected to have morphologies that are approximately: (i) E/S0, (ii) Sa, and (iii) Sb/Scd. The median luminosities of the hosts in the subsamples were all fairly similar: (i) $2.64\ L_{b_J}^*$, (ii) $2.25\ L_{b_J}^*$, and (iii) $2.11\ L_{b_J}^*$. The velocity dispersion profiles of all three samples decreased with radius and, moreover, $\sigma_v(r_p)$ was found to have a much higher amplitude and steeper decline for the satellites of early–type hosts than it did for the satellites of late–type hosts. See Figure 7. Although there is some difference in the median luminosities of the hosts in the subsamples, the difference is too small to have a significant effect on the velocity dispersion profiles. Therefore, the results of Brainerd [67] seem to indicate that early–type galaxies have deeper potential wells (and hence more massive halos) than late–type galaxies.

Previous work on the dependence of σ_v with projected radius using SDSS galaxies [65] and 2dFGRS galaxies [67] concluded that $\sigma_v(r_p)$ was consistent with an isothermal profile; i.e., $\sigma_v(r_p) =$ constant. In both of these investigations, the hosts and satellites were selected in a manner that was identical to that of Sample 3 in Prada et al. [27]. In both previous analyses, however, the number of hosts and satellites was significantly smaller than the more recent studies, and the formal error bars were correspondingly larger. In addition, the original analysis of SDSS host–satellite systems [65] neglected to account for the fact that the interloper fraction increases with radius, which would have biased measurements of σ_v at large r_p towards values which are higher than the actual satellite velocity dispersion at those

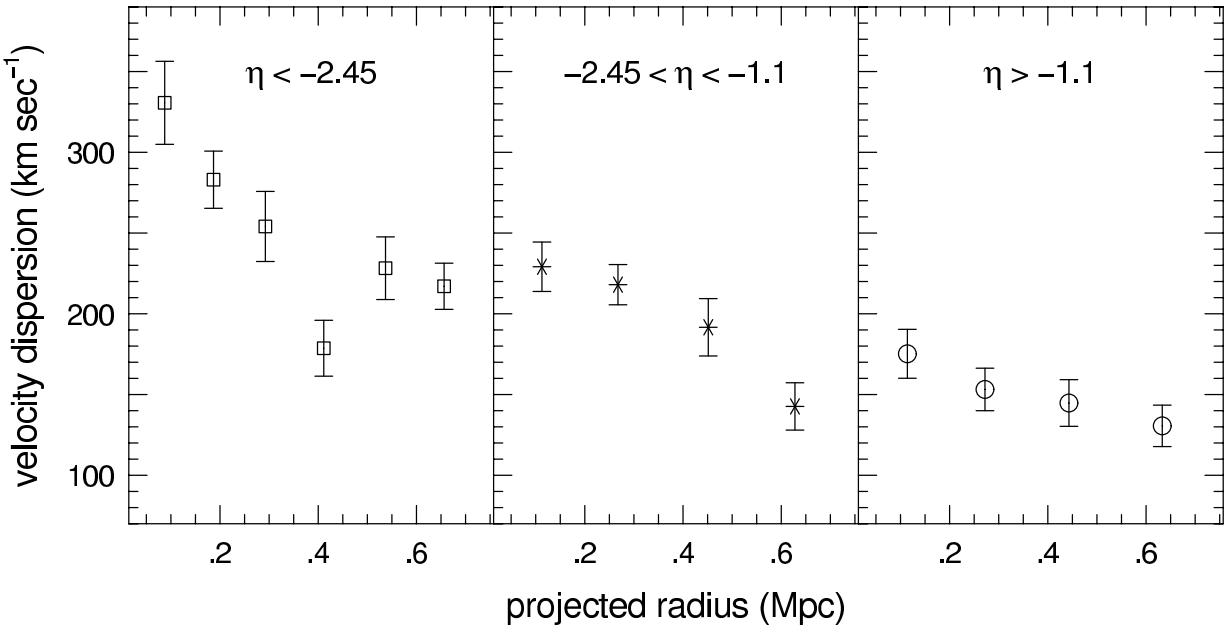

FIGURE 7. Velocity dispersion profiles for satellites in the final data release of the 2dFGRS as a function of the host spectral parameter, η [67]. The morphology of the hosts is expected to be roughly E/S0 in the left panel, Sa in the middle panel, and Sb/Scd in the right panel. The median luminosities of the subsamples in each of the panels is somewhat different, but the difference is too small to account for the differences in the velocity dispersion profiles. Here $h = 0.7$ has been adopted.

radii.

Even more recently, Conroy et al. [96] used satellites of $z \sim 0.8$ host galaxies in the DEEP2 survey to investigate $\sigma_v(r_p)$. DEEP2 (Deep Extragalactic Evolutionary Probe 2) is being carried out with the DEIMOS spectrograph at the Keck–II telescope, and will ultimately collect spectra of $\sim 60{,}000$ galaxies with redshifts of $0.7 \lesssim z \lesssim 1.4$ to a limiting magnitude of $R_{AB} = 24.1$ [97]. Unfortunately, the survey is still far from complete and only 61 isolated host galaxies (having a total of 75 satellites) were found in the current DEEP2 data. Because of this, the errors on $\sigma_v(r_p)$ are large, and formally $\sigma_v(r_p)$ for the DEEP2 galaxies is fitted well by a constant value: $\sigma_v(110\ h^{-1}\ \mathrm{kpc}) = 162^{+44}_{-30}$ km sec^{-1}, $\sigma_v(230\ h^{-1}\ \mathrm{kpc}) = 136^{+26}_{-20}$ km sec^{-1}, $\sigma_v(320\ h^{-1}\ \mathrm{kpc}) = 155^{+55}_{-38}$ km sec^{-1}. Therefore, isothermal halos for the DEEP2 galaxies cannot be ruled out at the moment. Conroy et al. [96] show, however, that their velocity dispersion measurements are consistent with expectations for NFW halos with virial masses in the range $3.5 \times 10^{12}\ h^{-1}\ M_\odot \leq M_{200} \leq 8.0 \times 10^{12}\ h^{-1}\ M_\odot$. This is in good general agreement with the results of Prada et al. [27], especially considering that the DEEP2 hosts are of order one magnitude brighter than the SDSS hosts (i.e., the virial mass implied for the halos of the brightest galaxies in the SDSS sample is $\sim 4 \times 10^{12} h^{-1} M_\odot$). At the moment, however, the DEEP2 data are too severely limited by small number statistics to place strong constraints on the nature of the dark matter halos of galaxies with redshifts of order unity.

HALO MASSES AND GALAXY MASS–TO–LIGHT RATIOS

Although it ought to be straightforward and even easy to compare the halo masses and galaxy mass–to–light ratios that are obtained from different studies, in practice it is rather like comparing persimmons to tomatoes; i.e., they are vaguely similar on the inside and outside, but they are definitely not interchangeable. The fundamental problem is that it is simply not possible to measure the "total" mass of a galaxy halo (since it is not possible to say where such a halo "ends") and, hence, all halo masses are simply masses that are contained within some physical radius of the center of the halo. Along those same lines, and given that velocity dispersion profiles of NFW halos decrease with radius, if one wants to compare the results of two investigations which have measured a velocity dispersion averaged over some large scale, it is important that those scales be *identical*. That is, suppose a single measurement of σ_v is made

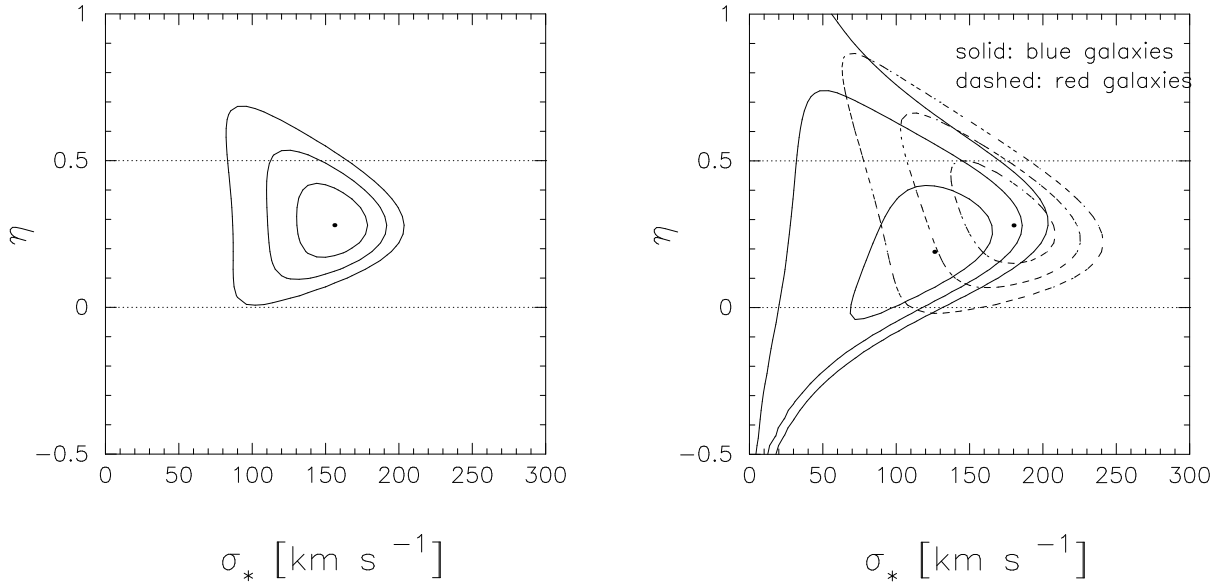

FIGURE 8. Isothermal sphere models for the galaxy–galaxy data from COMBO–17 [60]. Joint constraints (1σ, 2σ, and 3σ) on the velocity dispersion, σ_v^*, of the halos of L^* galaxies and the index of the Tully–Fisher/Faber–Jackson relation, η. Here the weak lensing signal has been averaged over scales $r_p \lesssim 150\,h^{-1}$ kpc. Left panels: all lenses, $\sigma_v^* = 156^{+18}_{-18}$ km sec^{-1}, $\eta = 0.28^{+0.12}_{-0.09}$. Right panels: red lenses (2579 galaxies, $\sigma^*_{v,\,\rm red} = 180^{+24}_{-30}$ km sec^{-1}) Left panels: blue lenses (9898 galaxies, $\sigma^*_{v,\,\rm blue} = 126^{+30}_{-36}$ km sec^{-1}). Figure kindly provided by Martina Kleinheinrich.

by averaging over scales $r < 100\,h^{-1}$ kpc in one study and a single measurement of σ_v is made by averaging over scales $r < 200\,h^{-1}$ kpc in another. If the second measurement of σ_v is lower than the first by some significant amount, that does not necessarily mean that the values are in disagreement. They would be in disagreement if both halos were isothermal spheres, but if the halos are NFW objects, then it is only to be expected that the second measurement would be lower than the first.

A more subtle problem is the definition of the "virial radius" in the context of NFW halos. While r_{200} was originally proposed as the radius at which the interior mass density is 200 times the critical mass density (e.g., [5], [6], [7]), it is not at all uncommon to find that investigators who have fit NFW models to their data have defined the virial radius as the radius at which the interior mass density is 200 times the mean mass density of the universe. Therefore, what is meant by a "virial mass" in the context of an NFW fit to data can (and does) vary from investigation to investigation, and a certain amount of care has to be taken when comparing such results. Despite the difficulties of comparing the conclusions of different studies, I will forge ahead because it is becoming clear that a consistent picture really is emerging on the topic of the masses of the halos of field galaxies, and their corresponding mass–to–light ratios. The weak lensing studies yield results that are by and large consistent with each other, and the dynamical studies seem to be in general agreement with the trends in the weak lensing data: the halos have masses that are consistent with expectations for galaxy–sized halos in CDM, and there are real, physical differences between halos surrounding (i) early–type and late–type galaxies and (ii) high–luminosity and low–luminosity galaxies.

M and M/L from Galaxy–Galaxy Lensing

In the case of galaxy–galaxy lensing, it is not possible at the moment to discriminate between shear profiles that are caused by NFW versus isothermal galaxy halos. Therefore, investigators will often choose one or the other to constrain the properties of the halos that are producing the lensing signal. In the case of isothermal sphere halos, the velocity dispersions of the lens galaxies used to model the observed signal are often chosen to scale as in eqn. (19) above, $(\sigma_v/\sigma_v^*) = (L/L^*)^\eta$, where again σ_v is the velocity dispersion of a halo that contains a galaxy of luminosity L, and σ_v^* is the velocity dispersion of the halo of an L^* galaxy. Hoekstra et al. [48] used this approach with their

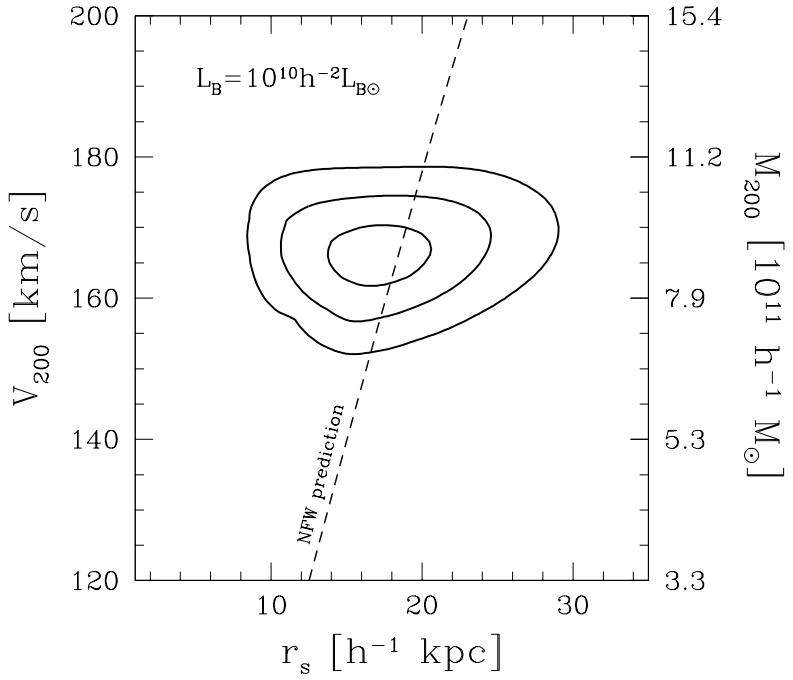

FIGURE 9. Constraints on the circular velocity at $r = r_{200}$ and the scale radius, r_s, for lenses in the RCS that have been modeled as having NFW–type halos [48]. Formally, the best–fitting values of the circular velocity, scale radius and virial mass are: $V_{200} = 162 \pm 8$ km sec^{-1}, $r_s = 16.2^{+3.6}_{-2.9}$ h^{-1} kpc, and $M_{200} = 8.4 \pm 1.1 \times 10^{11}$ h^{-1} $M_\odot$. Here r_{200} is defined as the radius at which the mean interior mass density of the halo is equal to $200\rho_c$. The dashed line shows the predictions of the NFW theory, in which V_{200} and r_{200} are not independent parameters. Figure kindly provided by Henk Hoekstra.

RCS data, as did Kleinheinrich et al. [60] with their COMBO–17 data. When all lenses and sources were used in the investigations, and when the lensing signal was averaged over an identical scale ($r \lesssim 350$ h^{-1} kpc), both the RCS and COMBO–17 results are in very good agreement with each other. In particular, Hoekstra et al. [48] find $\sigma_v^* = 136 \pm 8$ km sec^{-1}for an adopted value of $\eta = 0.3$, and Kleinheinrich et al. [60] find $\sigma_v^* = 138^{+18}_{-24}$ and $\eta = 0.34^{+0.18}_{-0.12}$. Further, Kleinheinrich et al. [60] find that there are clear differences in the halos surrounding "blue" galaxies (rest frame colors of $(U-V) \leq 1.15 - 0.31z - 0.08[M_V - 5\log h + 20]$) and those surrounding "red" galaxies (the remainder of the sample). That is, the red COMBO–17 lens galaxies have a higher velocity dispersion than the blue COMBO–17 lens galaxies, but both have a similar value of the index η above. See Figure 8.

In addition, Guzik & Seljak [16], Hoekstra et al. [48], and Kleinheinrich et al. [60] have all used NFW halos to model their lens galaxies, and all find very reasonable fits to their lensing signals. Further, the derived values of the NFW virial masses of the halos of L^* galaxies are in quite good agreement amongst these studies when they are determined in similar band passes (e.g., r) and with identical definitions of the virial radius [60]: $M^*_{\rm vir} = 8.96 \pm 1.59 \times 10^{11}\, h^{-1}\, M_\odot$ [16], $M^*_{\rm vir} = 8.4 \pm 0.7 \times 10^{11}\, h^{-1}\, M_\odot$ [48], and $M^*_{\rm vir} = 7.8^{+3.5}_{-2.7} \times 10^{11}\, h^{-1}\, M_\odot$ [60]. These are also in remarkably good agreement with the virial mass implied for the halos of L^* galaxies by the dynamical analysis of Prada et al. [27] (e.g., $M^*_{\rm vir} \sim 10 \times 10^{11} h^{-1} M_\odot$). Shown in Figure 9 are 1σ, 2σ and 3σ confidence limits on a joint–parameter fit of the circular velocity at r_{200}, V_{200}, and scale radius, r_s, for the lenses in the RCS data [48]. Note that in the analysis of the RCS data, V_{200} and r_s were allowed to vary freely, while, to within some scatter, these parameters are strongly correlated in the NFW theory (i.e., the NFW model is in essence specified by a single parameter). The dashed line in Figure 9 therefore shows the prediction for a strict adherence to the NFW theory (i.e., V_{200} and r_s are correlated appropriately), and the fact that the theoretical NFW line passes so well through the contours gives a certain amount of confidence that the NFW model is a very good fit to the data. Kleinheinrich et al. [60] find good fits of the NFW model to their data and, moreover, find that both the virial radii of the halos and the parameter η are dependent upon the rest frame colors of the galaxies, with red galaxies having a somewhat larger virial radius (and, hence, larger virial mass) than blue galaxies. See Figure 10. Here η is defined not as in eqn. (19), since the velocity dispersion is a function of

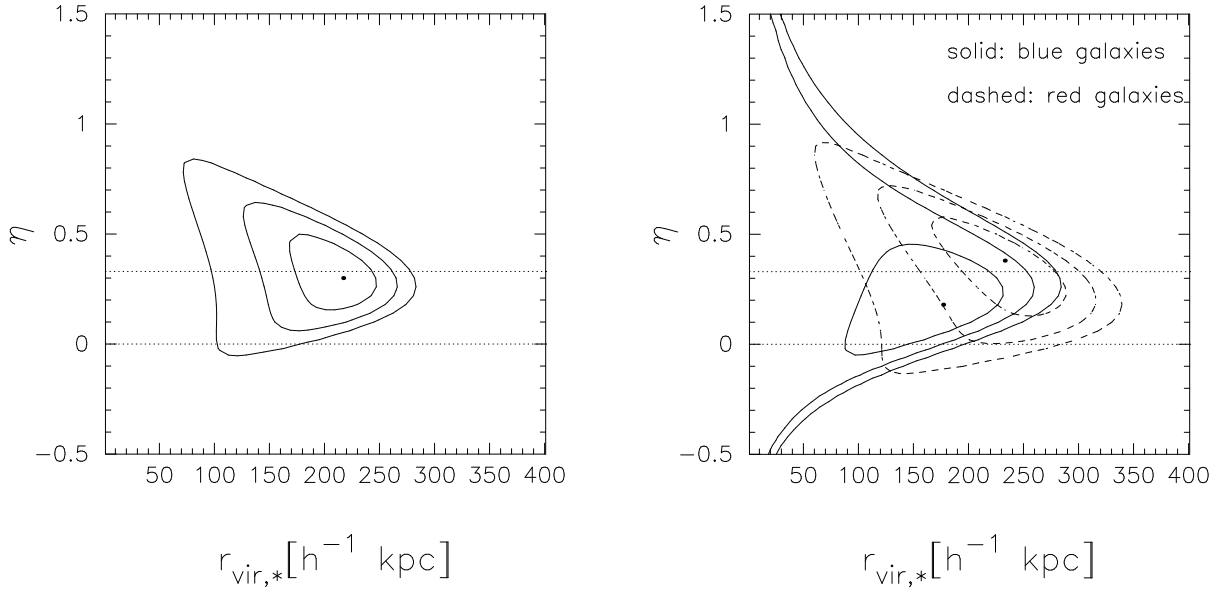

FIGURE 10. NFW halo models of the galaxy–galaxy lensing data from COMBO–17 [60]. Joint constraints (1σ, 2σ, and 3σ) on η and the virial radii of the halos of L^* galaxies are shown. Left panel: all lenses, $\eta = 0.30^{+0.16}_{-0.12}$, $r^*_{\rm vir} = 217^{+24}_{-32}\ h^{-1}$ kpc. Right panel: red lenses (2579 galaxies, $\eta = 0.38^{+0.16}_{-0.20}$, $r^*_{\rm vir} = 233^{+48}_{-48}\ h^{-1}$ kpc) versus blue lenses (9898 galaxies, $\eta = 0.18^{+0.16}_{-0.16}$, $r^*_{\rm vir} = 177^{+40}_{-56}\ h^{-1}$ kpc). Figure kindly provided by Martina Kleinheinrich.

projected radius in the NFW model, but rather it is defined as:

$$\frac{r_{\rm vir}}{r^*_{\rm vir}} = \left(\frac{L}{L^*}\right)^{\eta}, \tag{20}$$

in analogy to the Tully–Fisher and Faber–Jackson relations (see [60]). In this case, $r^*_{\rm vir}$ is the virial radius of the halo of an L^* galaxy, defined at 200 times the mean mass density of the universe. The variation of η with galaxy color and its implications for the mass–to–light ratios of the galaxies will be discussed below.

A particularly detailed study of the masses of lensing galaxies as a function of their color was carried out by Guzik & Seljak [16] for $\sim 3.5 \times 10^4$ lenses and $\sim 3.6 \times 10^6$ sources in the SDSS. All of the lens galaxies have spectroscopic redshifts in this case, and all of the halos were modeled as NFW objects in the context of the "halo model". In all 5 of the SDSS band passes, Guzik & Seljak [16] find that the virial masses of L^* ellipticals exceed those of L^* spirals though, unsurprisingly, the amount by which the masses of the ellipticals exceeds those of the spirals is a strong function of the band pass. In the redder bands, the masses of the ellipticals exceed those of the spirals by a factor of ~ 2 to ~ 2.5, while in g' the difference is a factor of ~ 6 and in u' the difference is close to an order of magnitude. Although it is difficult to make direct comparisons between the two studies (because of the differing definitions of the virial radius and the different definitions of the subsamples of galaxies), there is good general agreement between the results of Guzik & Seljak [16] and Kleinheinrich et al. [60]: when the galaxy–galaxy lensing signal is detected red band passes (e.g., R, r') and the lenses are modeled as NFW objects, the virial masses of red/early–type galaxies exceed those of blue/late–type galaxies by a factor of order 2.

In addition to the halos of early–type lenses having more mass than those of late–type lenses, the weak lensing work of Sheldon et al. [42] indicates that, again, in all 5 SDSS band passes, the projected excess surface mass density increases with the luminosity of the lens. Sheldon et al. [42] separated their $\sim 1.27 \times 10^5$ lenses into 3 magnitude bins (high, middle, and low luminosity), and the magnitude cuts differ for the different band passes. (See Table 2 of Sheldon et al. [42] for a complete list of the magnitude cuts as a function of band pass.) In the case of the r' data, the "high" luminosity galaxies have a mean absolute magnitude of -22.5, the "middle" luminosity galaxies have a mean absolute magnitude of -21.9, and the "low" luminosity galaxies have a mean absolute magnitude of -20.5. These mean luminosities correspond roughly to $4.5L^*$ ("high"), $2.7L^*$ ("middle") and $0.8L^*$ ("low") in the r' band.

In all cases, $\Delta\Sigma(r_p)$ for the "high" luminosity galaxies exceeds that of the "medium" and "low" luminosity galaxies, and for $r_p \lesssim 1\ h^{-1}$ Mpc, the difference corresponds to an approximately constant multiplicative factor. Specifically at $r_p \sim 100\ h^{-1}$ Mpc, however, $\Delta\Sigma$ for the high luminosity lenses in Sheldon et al. [42] exceeds that for the low luminosity lenses by a factors of ~ 3 in u', ~ 5 in g', ~ 5 in r', ~ 7 in i', and ~ 7 in z' (e.g., Figure 14 of Sheldon et al. [42]). Similar trends (i.e., higher projected excess surface mass density for more luminous lenses) were found by Seljak et al. [61] in their galaxy–galaxy lensing analysis of SDSS data.

Lastly, although there is reasonable agreement regarding the relative increase in mass for the halos of early–type lens galaxies versus late–type lens galaxies at fixed luminosity (i.e., L^*), there is some disagreement over the dependence of the mass–to–light ratio on the luminosity of the host. Specifically, in their redder bands Guzik & Seljak [16] find that the mass–to–light ratio goes as $M/L \propto L^{0.4\pm0.2}$ for $L > L^*$, suggestive of a mass–to–light ratio that increases with luminosity. Kleinheinrich et al. [60], however, find that M/L for their sample of lenses is more consistent with a constant value: $M/L \propto L^{-0.10^{+0.48}_{-0.36}}$. Both Guzik & Seljak [16] and Kleinheinrich et al. [60] agree, however, that the mass–to–light ratio of red/early–type L^* lens galaxies exceeds that of blue/late–type L^* lens galaxies by a factor of ~ 2 to ~ 2.5 in the redder bands.

M and M/L from Satellite Dynamics

In the 1990's, Zaritsky et al. [20] and Zaritsky & White [98] used the velocity differences between a small number of isolated spiral galaxies and their satellites to show that the halos of the spirals were massive and extended to large radii: $M(150\ h^{-1}\ \mathrm{kpc}) \sim 1$ to $2 \times 10^{12} h^{-1} M_\odot$. Moreover, Zaritsky et al. [20] found a somewhat curious result: the velocity difference between their 115 satellites and 69 hosts was independent of the inclination corrected H-I line width of the host and was, therefore, independent of the luminosity of the host (through, e.g., the Tully–Fisher relation). At fixed large radius, then, this would imply that M/L for the spiral hosts decreased as $M/L \propto L^{-1}$.

More recent investigations of halo masses and corresponding mass–to–light ratios from satellite dynamics have led to rather a large assortment of conclusions. McKay et al. [65] and Brainerd & Specian [66] used the dynamics of the satellites of SDSS galaxies and 2dFGRS galaxies, respectively, to constrain the dynamical masses of the halos of the host galaxies interior to a radius of $r = 260\ h^{-1}$ kpc. Both used an isothermal mass estimator of the form

$$M_{260}^{\mathrm{dyn}} = \frac{2.1\ r\ \sigma_v^2}{G}, \tag{21}$$

where σ_v is the line–of–sight velocity dispersion. Both felt this assumption was justified because both found that their velocity dispersion profiles were consistent with a constant value. In the case of McKay et al. [65], however, no correction for an increasing number of interlopers with projected radius was made and this may have led to an incorrect conclusion that $\sigma_v(r_p)$ was independent of r_p. In the case of Brainerd & Specian [66], the increasing number of interlopers at large r_p was taken into account, but only galaxies from the 100k data release of the 2dFGRS were used (i.e., roughly half as many galaxies as in the full data release), and although $\sigma_v(r_p)$ was consistent with a constant value in their data, the later analysis by Brainerd [67] showed that this was simply due to the rather large error bars in Brainerd & Specian [66]. This being the case, the mass–to–light ratios published by these two studies are suspect at some level, but it is unclear at the moment just how suspect they may actually be. That is, while it is true that the velocity dispersion profile of NFW halos decreases with radius, the fall–off in $\sigma_v(r_p)$ is not particularly sharp and it is not obvious how badly isothermal mass estimates of the form in eqn. (21), which are based on an average value of σ_v, will compare to proper NFW mass estimates.

Formally, McKay et al. [65] found that in all 5 SDSS band passes, M_{260}^{dyn}/L was roughly constant for $L > L^*$, and that the value of M_{260}^{dyn}/L was a strong function of the band pass (being systematically higher in the blue bands than in the red bands). Brainerd & Specian [66] found that for $L \gtrsim 2L^*$, M_{260}^{dyn}/L was a constant for dynamical analyses that included (i) all 809 hosts in their sample and (ii) 159 hosts that had been visually classified as early–type (E/S0). However, much like the results of Zartisky et al. [20], Brainerd & Specian [66] found that M_{260}^{dyn}/L decreased as $M_{260}^{\mathrm{dyn}}/L \propto L^{-1}$ for 243 hosts that had been visually classified as spirals. This latter result remains puzzling, and is certainly in need of further investigation with larger data sets.

In their analysis of the dynamics of the satellites of SDSS host galaxies, Prada et al. [27] found that the velocity dispersion of the satellites scaled with host luminosity as $\sigma_v \propto L^{0.3}$ (i.e., in good agreement with the local B–band Tully–Fisher relationship [99]) for satellites with projected radii $r_p < 120$ kpc. (Recall, too, that in this study $\sigma_v(r_p)$

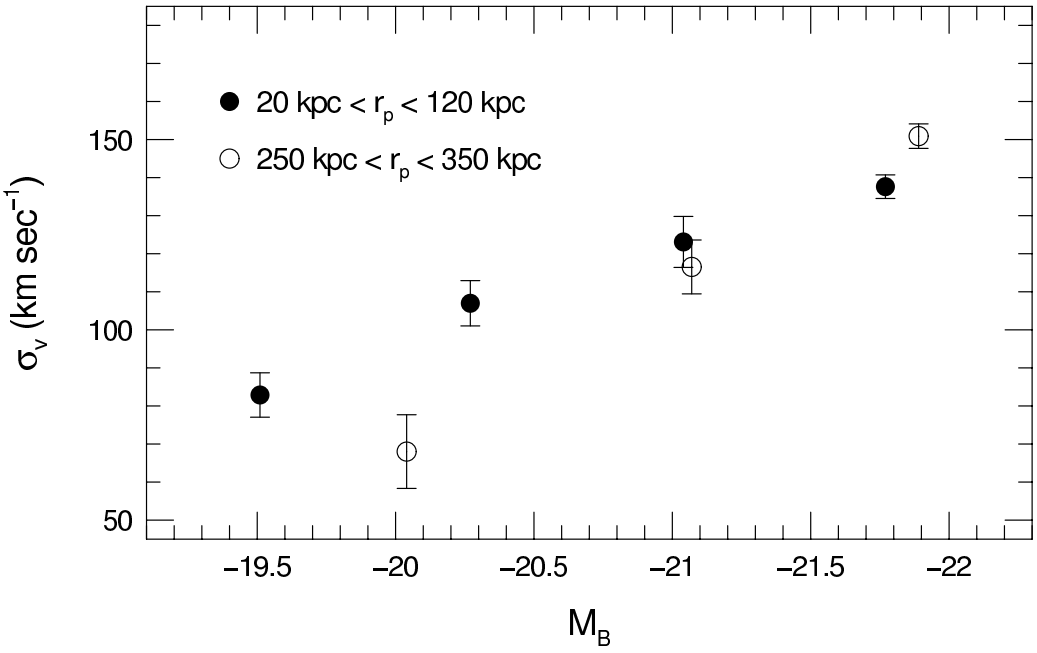

FIGURE 11. Dependence of satellite velocity dispersion on host absolute magnitude for SDSS galaxies [27]. Filled circles: σ_v computed using satellites with 20 kpc $\leq r_p \leq$ 120 kpc. Open circles: σ_v computed using satellites with 250 kpc $\leq r_p \leq$ 350 kpc. For small projected radii the velocity dispersion scales as $\sigma_v \propto L^{0.3}$, in good agreement with the local B–band Tully–Fisher relationship. For large projected radii $\sigma_v \propto L^{0.5}$. Here $h = 0.7$ has been adopted.

was specifically corrected for the increase in interlopers at large r_p.) In addition, Prada et al. [27] found that for satellites at large projected radius, 250 kpc $< r_p <$ 350 kpc, the velocity dispersion scaled with luminosity as $\sigma_v \propto L^{0.5}$ (i.e., steeper than expected from the Tully–Fisher relation). See Figure 11.

Similar to Prada et al. [27], Brainerd [67] also computed the dependence of the small–scale velocity dispersion of satellites on host luminosity. See Figure 12. Like Prada et al. [27], Brainerd [67] corrected for the fact that the interloper fraction is an increasing function of projected radius and overall, she found excellent agreement between the velocity dispersions of satellites with projected radii $r_p \leq 120$ kpc in the 2dFGRS and GIF simulations. The velocity dispersions of the 2dFGRS satellites were, however, seen to scale with host luminosity as $\sigma_v \propto L_{b_J}^{0.45\pm0.10}$, which is only marginally consistent with the results of Prada et al. [27] and the local *B*-band Tully–Fisher relationship.

Prada et al. [27] have shown (e.g., their Figure 12) that the dependence of the line of sight velocity dispersion on the virial mass of NFW halos scales as $\sigma_v \propto M_{\rm vir}^{0.38}$ for the case that σ_v is computed as an average over scales 20 kpc $\lesssim r_p \lesssim$ 100 kpc, and that $\sigma_v \propto M_{\rm vir}^{0.50}$ for the case that σ_v is computed at $r_p \sim 350$ kpc. Combining this with their results for the dependence of σ_v on L at different scales leads to the conclusion that on scales $r_p \lesssim 120$ kpc, $M_{\rm vir}/L \propto L^{-0.2}$ while on scales $r_p \sim 300$ kpc, $M_{\rm vir}/L$ is a constant. Similarly, if the halos of the 2dFGRS galaxies studied by Brainerd [67] are assumed to be NFW objects, the implication is that $M_{\rm vir}/L \propto L^{0.2^{+0.3}_{-0.1}}$ for the 2dFGRS hosts (again, computed on scales $r_p \lesssim 120$ kpc).

While it certainly cannot be said that there is a consensus from weak lensing and satellite dynamics as to the exact dependence of the galaxy mass–to–light ratio on L, it does seem to be the case that all of these studies point towards a dependence of $M_{\rm vir}/L$ on L that is, at most, rather weak. That is, with the notable exception of the Brainerd & Specian [66] result for late–type galaxies, all of the recent determinations of M/L for $L \gtrsim L*$ find that, to within 2σ, M/L is independent of L. In addition, when the weak lenses and host galaxies are each modeled as NFW objects, a fairly consistent value of the average virial mass of the halos of L^* galaxies is found: $\sim (8-10) \times 10^{11}\, h^{-1}\, M_\odot$. Further, it seems to be clear that both weak lensing and satellite dynamics indicate that the masses of the halos of early–type galaxies are larger than that of late–type galaxies, and that at fixed luminosity the mass–to–light ratios of early–type galaxies are larger than those of late–type galaxies.

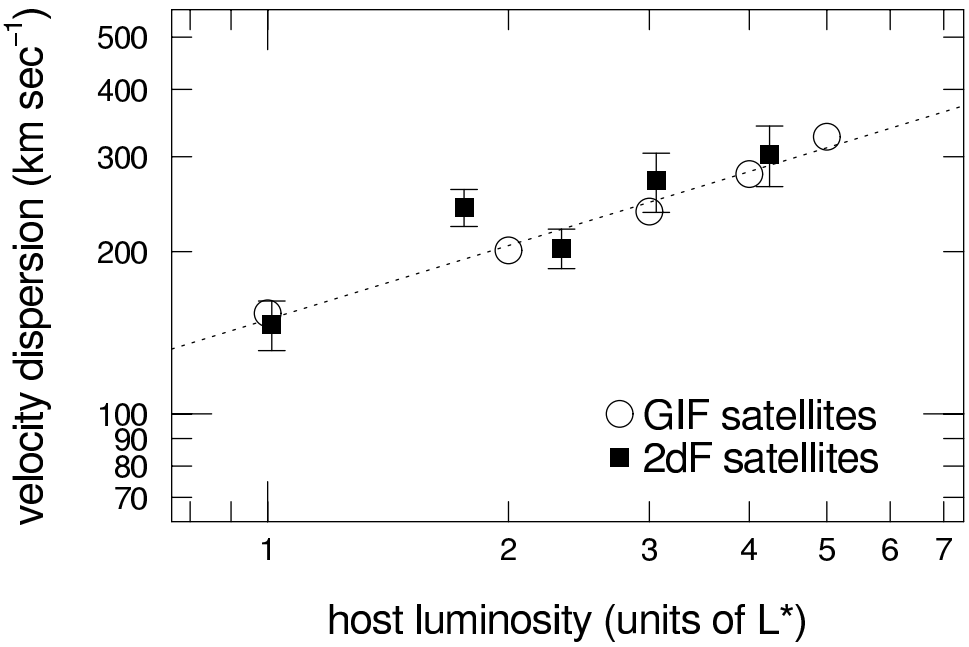

FIGURE 12. Dependence of satellite velocity dispersion on host luminosity for satellites with projected radii $r_p \leq 120$ kpc in both the 2dFGRS and the flat, Λ–dominated GIF simulation [67]. Dotted line shows $\sigma_v \propto L^{0.45}$.

NON–SPHERICAL HALOS

Although the simple isothermal sphere can reproduce the flatness of the rotation curves of the disks of spiral galaxies at large radii, there are both observational and theoretical arguments in favor of halos which are flattened, rather than spherical. Direct observational evidence for halo flattening that has come from studies of individual galaxies is somewhat scarce, however, owing to the fact that there are relatively few galaxies for which the shape of the halo potential can be probed directly. Nevertheless, the evidence for flattened halos of individual galaxies is diverse and includes such observations as the dynamics of polar ring galaxies, the geometry of X-ray isophotes, the flaring of HI gas in spirals, the evolution of gaseous warps, and the kinematics of Population II stars in our own Galaxy. In particular, studies of disk systems which probe distances of order 15 kpc from the galactic planes suggest that the ratio of shortest to longest principle axes of the halos is $c/a = 0.5 \pm 0.2$ (see, e.g., the comprehensive review by Sackett [100] and references therein). Studies of a number of strong lens galaxies have also suggested that the mass distributions of the lenses are not precisely spherical. For example, Maller et al. [101] found that, provided the disk mass is small compared to the halo mass, the halo of the spiral galaxy which lenses the quasar B1600+434 is consistent with $c/a = 0.53$. In addition, the 17 strong lens systems studied by Keeton, Kochanek & Falco [102] showed some preference for flattened mass distributions, although extremely flattened (i.e., "disky") mass distributions were ruled out. Finally, a recent analysis of the luminous halos of 1047 edge–on disk galaxies in the SDSS suggests that the old stellar populations of these galaxies consist of moderately flattened spheroids with axis ratios of $c/a \sim 0.6$ [103].

On the theoretical side, high–resolution simulations of dissipationless CDM models consistently produce markedly non–spherical galaxy halos with a mean projected ellipticity of $\varepsilon \sim 0.3$ (see, e.g., [104], [105]). It is known, however, that the dark matter will react to the condensation of baryons during galaxy formation (e.g., [106]) and that the resulting increase in the central density leads to a more spherical shape than if dissipation were not considered (e.g., [107]). Recent simulations performed by Kazantzidis et al. [108] show that on scales $r << r_{\rm vir}$, the effects of gas cooling cause a substantial circularization of the mass density profile, leading to a projected ellipticity of $\varepsilon \sim 0.4$ to 0.5 in the inner regions of the galaxy. However, on scales $r \sim r_{\rm vir}$ Kazantzidis et al. [108] find that the projected ellipticity is $\varepsilon \sim 0.3$. Since both the weak lensing shear and satellite dynamics are determined primarily by the large–scale mass distribution of the halos, the roundness of the mass distribution on small scales due to gas cooling should not have a dramatic effect. From a theoretical standpoint, therefore, it is not at all unreasonable to expect that galaxy–galaxy

lensing and satellite dynamics should reflect a significant flattening of the halos.

Evidence for Flattened Halos from Galaxy–Galaxy Lensing

Unlike a spherically–symmetric lens for which the gravitational lensing shear is isotropic about the lens center, the shear due to an elliptical lens is anisotropic about the lens center. Specifically, at a given angular distance, θ, from an elliptical lens, source galaxies which are located closer to the major axis of the mass distribution of the lens will experience greater shear than sources which are located closer to the minor axis (e.g., [8]). Noting this, Natarajan & Refregier [109] and Brainerd & Wright [110] modeled the dark matter halos of field galaxies as infinite singular isothermal ellipsoids and made rough estimates of the sizes of observational data sets which would be required to detect "anisotropic" galaxy–galaxy lensing and, hence, to constrain the net flattening of the halo population. Both studies concluded that, if the mean flattening of the halos is of order 0.3, then only a relatively modest amount of imaging data would be necessary to observe the effects of halo flattening on the weak lensing signal.

In estimating the amount of data that would be required to detect anisotropic galaxy–galaxy lensing, both Natarajan & Refregier [109] and Brainerd & Wright [110] made the simplifying assumption that each distant source galaxy is lensed by only one foreground galaxy. However, for a somewhat deep imaging survey ($I_{\rm lim} \sim 23$), the simulations of galaxy–galaxy lensing performed by Brainerd, Blandford & Smail [13] indicated that most of the galaxies with magnitudes in the range $22 \lesssim I \lesssim 23$ would have been lensed at a comparable level by two or more foreground galaxies. In a realistic data set, these multiple weak deflections might significantly affect the signal–to–noise that could be achieved when attempting to detect anisotropic galaxy–galaxy lensing. This motivated Wright & Brainerd [111] to carry out detailed Monte Carlo simulations of galaxy–galaxy lensing by flattened halos, including the effects of multiple weak deflections on the final images of distant galaxies.

Wright & Brainerd [111] showed that multiple weak deflections create systematic effects which could hinder observational efforts to use weak lensing to constrain the projected shapes of the dark matter halos of field galaxies. They modeled the dark matter halos of lens galaxies as truncated singular isothermal ellipsoids, and for an observational data set in which the galaxies had magnitudes in the range $19 \lesssim I \lesssim 23$, they found that multiple deflections resulted in strong correlations between the post–lensing image shapes of most foreground–background pairs of galaxies. Imposing a simple redshift cut during the analysis of the data set, $z_l < 0.5$ and $z_s > 0.5$, was sufficient to reduce the correlation between the final images of lenses and sources to the point that the expected anisotropy in the weak lensing signal was detectable via a straightforward average. Wright & Brainerd [111] concluded that previous theoretical calculations of weak lensing due to flattened halos had considerably underestimated the sizes of the observational data sets which would be required to detect this effect. In particular, for a multi–color survey in which the galaxies had apparent magnitudes of $19 \lesssim I \lesssim 23$ and the imaging quality was modest, Wright & Brainerd [111] found that a 4σ detection could be obtained with a survey area of order 22 sq. deg., provided photometric redshift estimates were made for the galaxies, the typical error in $z_{\rm phot}$ was $\lesssim 0.1$, and only source galaxies with azimuthal coordinates that were within $\pm 20^\circ$ of the lens symmetry axes were used in the data analysis.

To date, only one intrepid team of investigators has claimed a detection of flattened halos from observations of galaxy–galaxy lensing. In their analysis of the RCS galaxy–galaxy lensing signal Hoekstra, Yee & Gladders [48] took the approach of modeling the lens galaxies as having halos with ellipticities that scaled linearly with the ellipticity of the image of the lens: $\varepsilon_{\rm halo} = f\varepsilon_{\rm light}$. Further, they assumed that the major axis of the lens image was aligned with the major axis of the halo in projection on the sky. This is a sensible assumption provided the majority of the lenses are relaxed systems, and it is justified at least partially by the observations of Kochanek [112] who found that the major axes of the mass and light of strong lens galaxies were aligned to within $\sim 10^\circ$ in projection on the sky.

Hoekstra, Yee & Gladders [48] performed a maximum likelihood analysis and concluded that spherical halos (i.e., $f = 0$) could be ruled out at the 99.5% confidence level on the basis of their weak lensing signal (see Figure 13). Formally, Hoekstra, Yee & Gladders [48] found $f = 0.77^{+0.18}_{-0.21}$. Since the mean ellipticity of the lens images in their study was $\left\langle \varepsilon_{\rm light} \right\rangle = 0.414$, this implies a mean halo ellipticity of $\langle \varepsilon_{\rm halo} \rangle = 0.33^{+0.07}_{-0.09}$ and a projected axis ratio of $c/a = 0.67^{+0.09}_{-0.07}$. This is in excellent agreement with the expectations for CDM halos, as well as previous observational constraints on halo flattening obtained on large physical scales (see, e.g., [100]). While it may yet be a bit premature to call this result a "definitive" measurement of the flattening of field galaxy halos, it is certainly impressive and the statistics will only improve as weak lensing surveys become larger.

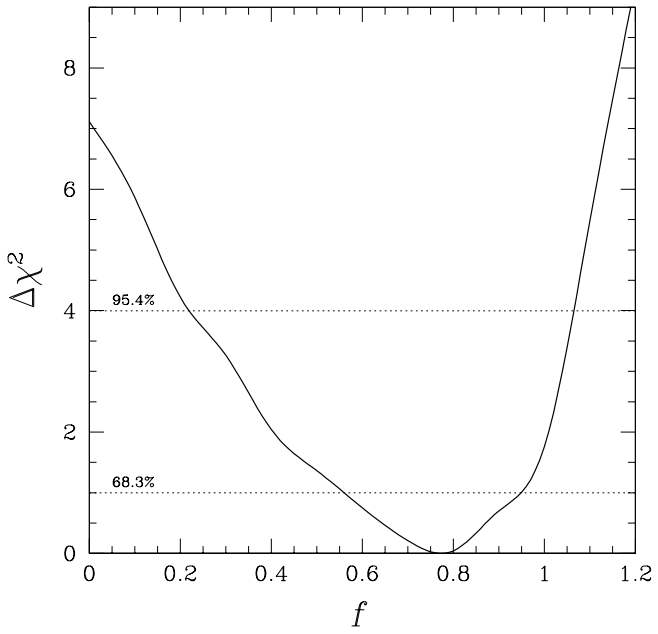

FIGURE 13. Confidence bounds with which spherical halos can be rejected on the basis of galaxy–galaxy lensing in the RCS [48]. Halos of lens galaxies were modeled as having ellipticities of $\varepsilon_{\rm halo} = f\varepsilon_{\rm light}$ and the principle axes of the halo mass were assumed to be aligned with the symmetry axes of the lens images in projection on the sky. Round halos, $f = 0$, are excluded at the 99.5% confidence level. Figure kindly provided by Henk Hoekstra.

Evidence for Flattened Halos from Satellite Galaxies

In the case of substantially flattened halos of host galaxies, one would naively expect that satellite galaxies would show a somewhat anisotropic distribution about the host. That is, barring possible effects due to infall rates and orbital decay, one would expect the satellites to have some preference for being located near to the major axis of the host's halo. Until very recently, however, such an observation had not been confidently made and, moreover, a preference for clustering of satellite galaxies along the *minor* axes of host galaxies has been reported at a statistically significant level by a handful of authors ([20], [68], [113]). The apparent alignment of satellite galaxies with the minor axes of the host galaxies is often referred to as the Holmberg effect and in the naive picture of satellite orbits in flattened potentials, observations of the Holmberg effect lead to the uncomfortable conclusion that not only is the halo mass flattened, but it is also anti–aligned with the luminous regions of the galaxy.

While one is tempted to dismiss the minor axis clustering of satellites observed by Zaritsky et al. [20] and Holmberg [113] as being due to some combination of selection biases and very small sample sizes, it is not easy to use this argument for the results of Sales & Lambas [68]. In their study, Sales & Lambas [68] selected hosts and satellites from the final data release of the 2dFGRS, with a resulting sample size of 1498 hosts and 3079 satellites. The satellites were constrained to be within projected radii $r_p \leq 500$ kpc of their host and to be within a velocity difference $|dv| < 500$ km sec^{-1}. Further, host images were required to have eccentricities of at least 0.1 in order that the orientation of their major axes be well–determined. When Sales & Lambas [68] searched their entire sample for anisotropies in the distribution of satellites about 2dFGRS hosts, their results were consistent with an isotropic distribution. However, when they restricted their sample to only hosts and satellites whose radial velocities differed by $|dv| < 160$ km sec^{-1}, an apparently strong detection of the Holmberg effect (i.e., minor axis clustering of the satellites) was found.

More recently, Brainerd [64] investigated the distribution of satellites about hosts in the second data release of the SDSS. She selected her samples using three different criteria: (1) the criteria used by Sales & Lambas [68] in their investigation of the Holmberg effect for 2dFGRS galaxies, (2) the criteria used by McKay et al. [65] and Brainerd & Specian [66] in their analyses of satellite dynamics in the SDSS and 2dFGRS, respectively, and (3) the selection

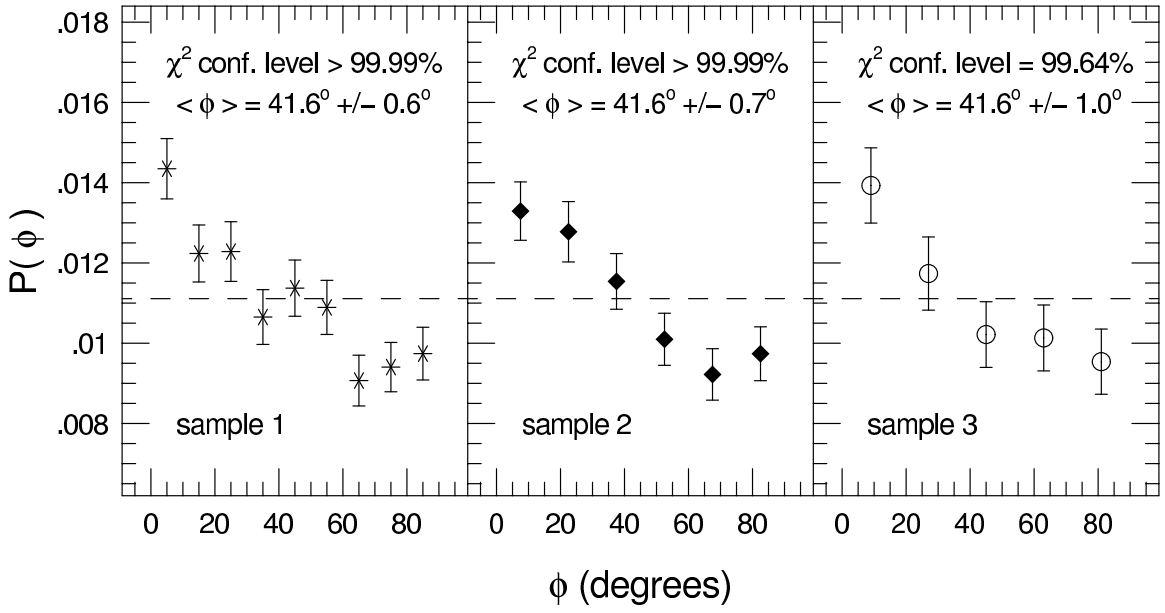

FIGURE 14. Normalized probability distribution of the location of satellite galaxies relative to the major axes of host galaxies in the second data release of the SDSS [64]. Dashed line shows the expectation for an isotropic distribution. Formal confidence levels at which isotropic distributions can be rejected via χ^2 tests are shown in each panel. Also shown is $\langle\phi\rangle$, the mean value of the angle between the major axis of the host galaxy and the direction vector that connects the centroids of the host and satellite.

criteria used by Zartisky et al. [20] in their investigation of the Holmberg effect. In addition, Brainerd [64] restricted the analyses to hosts with ellipticities $\varepsilon \geq 0.2$ and satellites that were found within a projected radius of 500 kpc. The three selection criteria lead to samples of: (1) 1351 hosts and 2084 satellites, (2) 948 hosts and 1294 satellites, and (3) 400 hosts and 658 satellites respectively.

In all three samples, Brainerd [64] found that the distribution of satellites about their hosts was inconsistent with an isotropic distribution. Formally, when a Kolmogorov–Smirnov test was applied to the distribution of satellite locations, an isotropic distribution was rejected at a confidence level of $> 99.99\%$ for sample 1, $> 99.99\%$ for sample 2, and 99.89% for sample 3. Further, the mean angle between the major axis of the host and the direction vector on the sky that connected the centroids of the hosts and satellites was found to be $\langle\phi\rangle = 41.6^\circ \pm 0.6^\circ$ for sample 1, $\langle\phi\rangle = 41.6^\circ \pm 0.7^\circ$ for sample 2, and $\langle\phi\rangle = 41.6^\circ \pm 1.0^\circ$ for sample 3. That is, a clear anisotropy in the distribution of satellites about the hosts was seen, and the satellites showed a preference for being aligned with the *major* axis of the host rather than the minor axis (see Figure 14). In addition, Brainerd [64] investigated the dependence of $\langle\phi\rangle$ with projected radius on the sky and found that the majority of the anisotropy arose on small scales ($\lesssim 200$ kpc) in all three samples (see Figure 15). In other words, the anisotropy was detected on physical scales that are comparable to the expected virial radii of large, bright galaxies. On scales much larger than the expected virial radii of galaxy–sized halos ($r_p \sim 400$ kpc to 500 kpc), the distribution of satellites about the SDSS hosts was consistent with an isotropic distribution at the 1σ level.

Aside from the Brainerd [64] claim of "planar" (rather than "polar") alignment of satellites with the symmetry axes of their hosts, there has been only one other similar claim. Valtonen, Teerikorpi & Argue [114] found a tendency for compact satellites to be aligned with the major axes of highly–inclined disk galaxies; however, their sample consisted of only 7 host galaxies. Although it is extremely tempting to accept its veracity based upon an intuitive sense that planar alignment of satellites is more dynamically sensible than polar alignment, it is clear that the Brainerd [64] result is badly in need of independent confirmation.

Sales & Lambas [68] used a data set of very similar size (and in one case identical selection criteria) to that of Brainerd [64] yet did not detect any anisotropy in the satellite distribution when they analysed their entire sample. Why this is the case remains a mystery at the moment, but it may be attributable to a combination of two things. First, the velocity errors in the 2dFGRS are typically larger than those in the SDSS (~ 85 km sec^{-1}versus ~ 20 km sec^{-1}to ~ 30 km sec^{-1}). At some level, this would lead to a higher fraction of interlopers (i.e., false satellites) in the Sales & Lambas [68] sample than in the Brainerd [64] samples. Second, van den Bosch et al. [115] found that when they

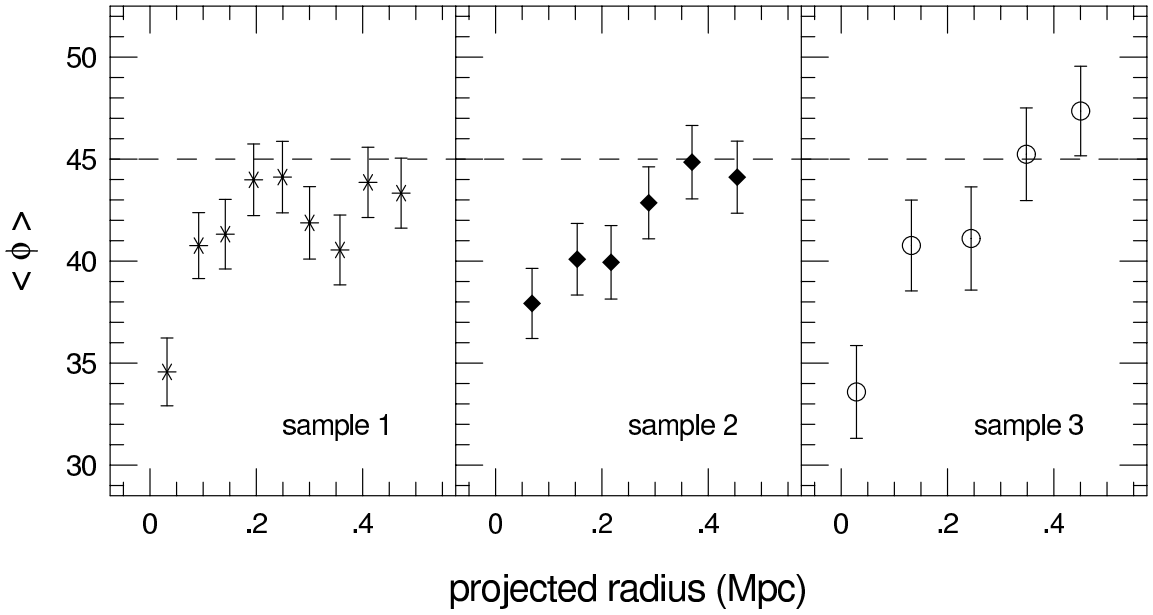

FIGURE 15. Mean orientation of satellite galaxies with respect to the major axes of the hosts as a function of the projected radius for galaxies in the second data release of the SDSS [64]. Dashed line shows the expectation for an isotropic distribution. Here $h = 0.7$ has been adopted.

combined mock redshift surveys with the 2dFGRS, there was a clear absence of satellites at small projected radii in the 2dFGRS. Since the majority of the anisotropy seen by Brainerd [64] appears to come primarily from small scales, it could be that Sales & Lambas [68] simply had too few pairs of hosts and satellites at small separations to detect the anisotropy. Any lack of host–satellite pairs in the 2dFGRS data, however, does not explain why a Holmberg effect was detected by Sales & Lambas [68] when they restricted their analysis to host–satellite pairs with $|dv| < 160$ km sec^{-1}. When Brainerd [64] imposed the same restriction on her sample 1 (i.e., the sample selected using the Sales & Lambas [68] selection criteria), she found that the satellites with $|dv| < 160$ km sec^{-1}displayed an anisotropy that was identical to that of the full sample: a clear alignment of the satellites with the host major axes. The cause of this discrepancy is not at all obvious. It may in part be attributable to the fact that a value of $|dv| = 160$ km sec^{-1}is comparable to the error in a typical measurement of $|dv|$ for hosts and satellites in the 2dFGRS. Also, work by van den Bosch et al. [69] suggests that the interloper fraction is substantially higher for host–satellite pairs with low values of $|dv|$ than it is for host–satellite pairs with high values of $|dv|$. It could, therefore, be possible that the Sales & Lambas [68] sample with $|dv| < 160$ km sec^{-1}is heavily contaminated with interlopers and some strange, unknown selection bias is giving rise to their signal.

Finally, it is worth notating that not only are the observational conclusions about the distribution of satellite galaxies particularly muddy at the moment, so too are the theoretical conclusions. Zaritsky et al. [20] compared their observed Holmberg effect with high–resolution CDM simulations and were unable to recover their observations. Peñarrubia et al. [116] investigated both polar and planar orbits of satellites inside a massive, flattened dark matter halo and found that the planar orbits decayed more quickly that the polar orbits. They therefore suggest that such differences in orbital decay rates could be the origin of the Holmberg effect. Abadi et al. [117] suggest that the Holmberg effect could be caused by the cumulative effects of accretion of satellites by the primary. However, Knebe et al. [118] found that the orbits of satellites of primary galaxies in cluster environments were located preferentially within a cone of opening angle 40° (i.e., planar alignment, not polar). Since the structure of cold dark matter halos is essentially independent of the mass scale of the halo (e.g., [119], [120]), the implication of this result would be a preference for the satellites of isolated galaxies to be aligned with the major axis of the host. All of this in mind, perhaps the only answer to the question “Are either the Sales & Lambas [68] or Brainerd [64] observations of anisotropic satellite distributions consistent with galaxy halos in a CDM universe?” is, for now, “Maybe”.

SUMMARY

There has been a long period of time over which it has been perfectly acceptable to write papers on investigations into the nature of the dark matter halos of field galaxies that begin with a statement along the lines of "Although modern theories of galaxy formation posit that all large galaxies reside within massive halos of dark matter, the characteristic properties of those halos (e.g., mass, radial extent, and shape) are not well–constrained by the current observations". That time is now coming to an end. The wealth of data that has been acquired in recent years is truly beginning to place strong, direct constraints on the dark matter halos of field galaxies.

Weak lensing and satellite dynamics have proven themselves to be excellent probes of the gravitational potentials of large, bright galaxies on physical scales $r \gtrsim 100\ h^{-1}$ kpc. While one might be skeptical and discount the results that come from one technique or the other, the fact that both are yielding consistent constraints cannot be ignored. Both weak lensing and satellite dynamics lead to statistical constraints on the halo population as a whole, rather than constraints on any one particular galaxy halo, and it is especially the acquisition of extremely large data sets that has allowed these techniques to begin to fulfill their promise of mapping out the gravitational potentials associated with large, massive halos. Weak lensing and satellite dynamics have inherent advantages and disadvantages, but since their systematic errors and selection biases are completely uncorrelated, they are extremely complementary to each other. At least at the moment, when strong constraints are only just beginning to emerge from each technique, this complementarity is very reassuring.

Based upon my own critical, and hopefully unbiased, reading of the recent literature, I think it is fair to say that, both individually and in combination, weak lensing and satellite dynamics are pointing toward the following scenario for the nature of large, bright field galaxies and their halos:

- The dark matter halos are well-characterized by NFW–type objects in terms of their gravitational properties. The dynamics of satellite galaxies strongly prefer NFW halos to isothermal halos.
- The virial masses that are inferred for large field galaxies are in good agreement with the predictions for galaxy–mass halos in the context of cold dark matter. Specifically, the virial mass of the halo of an "average" L^* galaxy is in the range $(8-10)\times 10^{11}h^{-1}M_\odot$ when NFW profiles are fit to the data.
- There are clear differences in the depths of the potential wells of the halos that surround galaxies of differing morphology and differing intrinsic luminosity. Specifically, the virial masses of the halos of L^* ellipticals exceed those of L^* spirals by a factor of at least 2. The actual value of the mass excess depends upon details of the data and its analysis. In addition, the virial masses of the halos of high luminosity galaxies exceed those of low luminosity galaxies. Again, however, the amount by which they differ depends upon details of the data and its analysis.
- Averaged over all galaxies with $L \gtrsim L^*$, the mass–to–light ratio computed on scales larger than the optical radii of the galaxies is, at most, weakly–dependent upon the luminosity of the galaxy. At the 2σ level, the mass–to–light ratio of the average galaxy with $L \gtrsim L^*$ is consistent with a constant value.
- The dark matter halos are flattened, rather than spherical, and the degree of flattening on large scales (~ 100 kpc to ~ 200 kpc) is consistent with the predictions of cold dark matter.

It is worth noting that the above list comes from quite a diverse set of data. In particular, the data are spread over a wide range in redshift. With the exception of preliminary data from DEEP2, the satellite dynamics studies have median redshifts of $z_{\rm med} \sim 0.07$. The weak lenses in the SDSS data have a median redshift of $z_{\rm med} \sim 0.16$ and the weak lenses in the RCS and COMBO–17 data have considerably higher redshifts, $z_{\rm med} \sim 0.4$. Since it is clear that the field galaxy population has evolved since $z \sim 0.5$, it is not entirely fair to lump the results from all of these studies together, and I think the big challenge to the weak lensing community in particular will be to eventually place constraints on the evolution of field galaxies and their halos from, say, $z \sim 1$ to the present.

Nevertheless, I think we have reached a particularly gratifying time in which we are really being able to measure some of the fundamental properties of dark mater halos on physical scales that extend well beyond the visible images of the galaxies at their centers. A remarkably consistent picture of the large–scale gravitational properties of the halos is emerging from the observations and, at least for now, that picture seems entirely in accord with a cold dark matter universe.

ACKNOWLEDGMENTS

I am deeply indebted to Henk Hoekstra, Martina Kleinheinrich, and Erin Sheldon for their help with the preparation of numerous figures at a time when they all had much more important things do to, and to Tom Peterson, without whose indulgence and encouragement this article would probably never have been written. Support under NSF contracts AST–0098572 and AST–0406844 is also gratefully acknowledged.

REFERENCES

1. Mathews, W. G. & Brighenti, F. 2003, ARAA, 41, 191
2. Sofue, Y. & Rubin, V. 2001, ARAA, 39, 137
3. Fich, M. & Tremaine, S. 1991, ARAA, 29, 409
4. de Zeeuw, T. & Franx, M. 1991, 29, 239
5. Navarro, J. F., Frenk, C. S. & White, S. D. M. 1995, MNRAS, 275, 720
6. Navarro, J. F., Frenk, C. S. & White, S. D. M. 1996, ApJ, 462, 563
7. Navarro, J. F., Frenk, C. S. & White, S. D. M. 1997, ApJ, 490, 493
8. Schneider, P., Ehlers, J. & Falco, E. E. 1992, *Gravitational Lensing*, (Berlin: Springer–Verlag)
9. Mellier, Y. 1999, ARAA, 37, 127
10. Bartelmann, M. & Schneider, P. 2001, Physics Reports, 340, 291
11. Wittman, D. 2002, in *Gravitational Lensing: An Astrophysical Tool*, Lecture Notes in Physics, eds. F. Courbin & D. Minniti (Springer–Verlag: Berlin, Heidelberg), 55
12. Narayan, R. & Bartelmann, M. 1999, in *Formation of Structure in the Universe*, eds. A. Dekel & J. P. Ostriker (Cambridge: Cambridge University Press), 360
13. Brainerd, T. G., Blandford, R. D. & Smail, I. 1996, ApJ, 466, 623
14. Brainerd, T. G. & Blandford, R. D. 2002, in *Gravitational Lensing: An Astrophysical Tool*, Lecture Notes in Physics, eds. F. Courbin & D. Minniti (Springer–Verlag: Berlin, Heidelberg), 96
15. Brainerd, T. G. 2005, in *The Impact of Gravitational Lensing on Cosmology*, proceedings of IAU Symposium 225, eds. Y. Mellier & G. Meylan, in press, `http://arxiv.org` e–Print archive, astro–ph/0409374
16. Guzik, J. & Seljak, U. 2002, MNRAS, 335, 311
17. Tyson, J. A. 1985, Nature, 316, 799
18. Bernstein, G. M. & Norberg, P. 2002, AJ, 124, 733
19. Hirata, C. M., Mandelbaum, R., Seljak, U., Guzik, J., Padmanabhan, N., Blake, C., Brinkmann, J., Budávari, T., Connolly, A., Csabai, I., Scranton, R. & Szalay, A. S. 2004, MNRAS, 353, 529
20. Zaritsky, D., Smith, R., Frenk, C. S. & White, S. D. M. 1997, ApJ, 478, L53
21. Wolf, C., Dye, S., Kleinheinrich, M., Rix, H.–W., Meisenheimer, K. & Wisotzki, L. 2001, AA, 377, 442
22. Wolf, C., Meisenheimer, K., Rix, H.–W., Borch, A., Dye, S. & Kleinheinrich, M. 2003, AA, 401, 73
23. Wolf, C., Meisenheimer, K., Kleinheinrich, M., Borch, A., Dye, S., Gray, M., Wisotzki, L., Bell, E., Rix, H.–W., Ciamatti, A., Hasinger, G. & Szokoly, G. 2004, AA, 421, 913
24. Kleinheinrich, M., Schneider, P., Erben, T., Schirmer, M., Rix, H.–W. & Meisenheimer, K. 2004, in *Gravitational Lensing: A Unique Tool for Cosmology*, ASP Conf. Series, eds. D. Valls–Gabaud & J.–P. Kneib (in press), `http://arxiv.org` e–Print archive, astro–ph/0304208
25. Yee, H. K. C. & Gladders, M. D. 2002, in *AMiBA 2001: High–z Clusters, Missing Baryons, and CMB Polarization*, ASP Conf. Series vol. 257, eds. L.–W. Chen, K.–W. Ng & U.–L. Pen, 109
26. Gladders, M. D. & Yee, H. K. C. 2004, submitted to ApJ Supplements
27. Prada, F., Vitvitska, M., Klypin, A., Holtzman, J. A., Schelgel, D. J., Grebel, E., Rix, H.–W., Brinkmann, J., McKay, T. A. & Csabai, I. 2003, ApJ, 598, 260
28. Tegmark, M., Blanton, M. R., Strauss, M. A., Hoyle, F., Schlegel, D., Scoccimarro, R., Vogeley, M. S., Weinberg, D., Zehavi, I., Berlind, A. and 55 coauthors, 2004, ApJ, 606, 702
29. York, D. G., Adelman, J., Anderson, J. E., Jr., Anderson, S. F., Annis, J., Bahcall, N. A., Bakken, J. A., Barkhouser, R., Bastian, S., Berman, E., and 134 coauthors, 2000, AJ, 120, 1579
30. Strauss, M. A., Weinberg, D. H, Lupton, R. H., Narayanan, V. K., Annis, J., Bernardi, M., Blanton, M., Burles, S., Connolly, A. J., Dalcanton, J., and 26 coauthors, 2002, AJ, 124, 1810
31. Fukugita, M., Ichikawa, T., Gunn, J. E., Doi, M., Shimasaku, K. & Schneider, D.P. 1996, AJ, 111, 1748
32. Hogg, D. W., Finkbeiner, D. P., Schlegel, D. J. & Gunn, J. E. 2001, AJ, 122, 2129
33. Smith, J. A., Tucker, D. L, Kent, S., Richmond, M. W., Fukugita, M., Ichikawa, T., Ichikawa, S., Jorgensen, A. M., Uomoto, A., Gunn, J. E., and 12 coauthors, 2002, AJ, 123, 212
34. Maddox, S. J., Efstathiou, G., Sutherland, W. J. & Loveday, J. 1990a, MNRAS, 243, 692
35. Maddox, S. J., Efstathiou, G., Sutherland, W. J. & Loveday, J. 1990b, MNRAS, 246, 433
36. Colless, M. M., Dalton, G. B., Maddox, S. J., Sutherland, W. J., Norberg, P., Cole, S. M., Bland–Hawthorn, J., Bridges, T. J., Cannon, R. D., Collins, C. A., Couch, W. J., Cross, N., Deeley, K., De Propris, R., Driver, S. P.,

Efstathiou, G., Ellis, R. S., Frenk, C. S., Glazebrook, K., Jackson, C. A., Lahav, O., Lewis, I. J., Lumsden, S., Madgwick, D. S., Peacock, J. A., Peterson, B. A., Price, I. A., Seaborne, M. & Taylor, K. 2001, MNRAS, 328,1039
37. Colless, M., Peterson, B. A., Jackson, C., Peacock, J. A., Cole, S., Norberg, P., Baldry, I. K., Baugh, C. M., Bland–Hawthorn, J., Bridges, T., Cannon, R., Collins, C., Couch, W., Cross, N., Dalton, G., De Propris, R., Driver, S. P., Efstathiou, G., Ellis, R. S., Frenk, C. S., Glazebrook, K., Lahav, O., Lewis, I., Lumsden, S., Maddox, S., Madgwick, D., Sutherland, W. & Taylor, K. 2003, http://arxiv.org e–Print archive, astro–ph/0306581
38. Norberg, P., Cole, S., Baugh, C. M., Frenk, C. S., Baldry, I., Bland–Hawthorn, J., Bridges, T., Cannon, R., Colless, M., Collins, C. A., Couch, W. J., Dalton, G. B., De Propris, R., Driver, S. P., Efstathiou, G., Ellis, R. S., Glazebrook, K., Jackson, C. A., Lahav, O., Lewis, I. J., Lumsden, S., Maddox, S. J., Madgwick, S. J., Peacock, J. A., Peterson, B. A., Sutherland, W. J. & Taylor, K. 2002, MNRAS, 336, 907
39. Blandford, R. D., Saust, A. B., Brainerd, T. G. & Villumsen, J. V. 1991, MNRAS, 251, 600
40. Kaiser, N., Squires, G. & Broadhurst, T. 1995, ApJ, 449, 460
41. Bernstein, G. M. & Jarvis, M. 2002, AJ, 123, 583
42. Sheldon, E. S., Johnston, D. E., Frieman, J. A., Scranton, R., McKay, T. A., Connolly, A. J., Budavári, T., Zehavi, I., Bahcall, N. A., Brinkmann, J. & Fukugita, M. 2004, ApJ, 127, 2544
43. Goldberg, D. M. & Bacon, D. J. 2004, submitted to ApJ, http://arxiv.org e–Print archive, astro–ph/0406376
44. Goldberg, D. M. & Natarajan, P. 2002, ApJ, 564, 65
45. Wittman, D., Tyson, J. A., dell'Antonio, I. P., Becker, A., Margoniner, V., Cohen, J. G., Norman, D., Loomba, D., Squires, G., Wilson, G., and 12 coauthors, 2002, SPIE, 4836, 73
46. Tyson, J. A., Valdes, F., Jarvis, J. F. & Mills, A. P., Jr. 1984, ApJ, 281, L59
47. Tyson, J. A. 1987, in *Dark Matter in the Universe*, proceedings of IAU Symposium 117, eds. J. Kormendy & G. R. Knapp (D. Reidel; Dordrecht)
48. Hoekstra, H., Yee, H. K. C. & Gladders, M. 2004, ApJ, 606, 67
49. Griffiths, R. E., Casertano, S., Im, M. & Ratnatunga, K. 1996, MNRAS, 282, P1159
50. dell'Antonio, I. P. & Tyson, J. A. 1996, ApJ, 473, L17
51. Hudson, M. J., Gwyn, S. D. J., Dahle, H. & Kaiser, N. 1998, ApJ, 503, 531
52. Ebbels, T. 1998, *Galaxy Evolution from Gravitational Lensing Studies with the Hubble Space Telescope*, PhD Thesis, Univ. of Cambridge
53. Fischer, P., McKay, T. A., Sheldon, E., Connolly, A., Stebbins, A., Frieman, J. A., Jain, B., Joffre, M., Johnston, D., Bernstein, G., and 30 coauthors 2000, AJ, 120, 1198
54. Hoekstra, H. 2000, *A Weak Lensing Study of Massive Structures*, PhD Thesis, Univ. of Groningen
55. Jaunsen, A. O. 2000, *Gravitational Lensing and Gamma Ray Bursts as Cosmological Probes*, PhD Thesis, Univ. of Oslo
56. McKay, T. A., Sheldon, E. S., Racusin, J., Fischer, P., Seljak, U., Stebbins, A., Johnston, D., Frieman, J. A., Bahcall, N., Brinkmann, J., Csabai, I., Fukugita, M., Hennessy, G. S., Ivezic, Z., Lamb, D. Q., Loveday, J., Lupton, R. H., Munn, J. A., Nichol, R. C., Pier, J. R. & York, D. G. 2001, http://arxiv.org e–Print archive, astro–ph/0108013
57. Smith, D. R., Bernstein, G. M., Fischer, P. & Jarvis, M. 2001, ApJ, 551, 643
58. Wilson, G., Kaiser, N., Luppino, G. A. & Cowie, L. L. 2001, ApJ, 555, 572
59. Hoekstra, H., Franx, M., Kuijken, K., Carlberg, R. G. & Yee, H. K. C. 2003, MNRAS, 340, 609
60. Kleinheinrich, M., Rix, H.–W., Schneider, P., Erben, T., Meisenheimer, K., Wolf, C. & Schirmer, M. 2005, in *The Impact of Gravitational Lensing on Cosmology*, proceedings of IAU Symposium 225, eds. Y. Mellier & G. Meylan (in press), http://arxiv.org e–Print archive, astro–ph/0409320
61. Seljak, U., Makarov, A., Mandelbaum, R., Hirata, C. M., Padmanabhan, N., McDonald, P., Blanton, M. R., Tegmark, M., Bahcall, N. A. & Brinkmann, J. 2004, submitted to PRD, http://arxiv.org e–Print archive, astro–ph/0406594
62. Giralda–Escudé, J. 1991, ApJ, 370, 1
63. Kaiser, N., Fahlman, G. & Woods, D. 1994, in *Clusters of Galaxies*, ed. F. Durret (Gif-sur-Yvette: Ed. Frontières)
64. Brainerd, T. G., 2004, submitted to ApJ Letters, http://arxiv.org e–Print archive, astro–ph/0408559
65. McKay, T. A., Sheldon, E. S., Johnston, D., Grebel, E. K., Prada, F., Rix, H.–W., Bahcall, N. A., Brinkmann, J., Csabai, I., Fukugita, M., Lamb, D. Q. & York, D. G. 2002, ApJ, 571, L85
66. Brainerd, T. G. & Specian, M. A. 2003, ApJ, 593, L7
67. Brainerd, T. G., 2004, submitted to ApJ, http://arxiv.org e–Print archive, astro–ph/0409381
68. Sales, L. & Lambas, D. G. 2004, MNRAS, 348, 1236
69. van den Bosch, F. C., Yang, X., Mo, H. J. & Norberg, P. 2004, http://arxiv.org e–Print archive, astro–ph/0406246
70. Bartelmann, M., Huss, A., Colberg, J. M., Jenkins, A., & Pearce, F. R. 1998, A&A, 330, 1
71. Thomas, P. A., Colberg, J. M., Couchman, H. M. P., Efstathiou, G. P., Frenk, C. S., Jenkins, A. R., Nelson, A. H., Hutchings, R. M., Peacock, J. A., Pearce, F. R. & White, S. D. M. 1998, MNRAS, 296, 1061
72. Kravtsov, A. V., Klypin, A. A., & Khokhlov, A. M. 1997, ApJS, 111, 73
73. Tormen, G., Bouchet, F. R. & White, S. D. M. 1997, MNRAS, 286,865
74. Ghigna, S., Moore, B., Governato, F., Lake, G., Quinn, T., & Stadel, J. 1998, MNRAS, 300, 146

75. Moore, B., Governato, F., Quinn, T. & Stadel, J. 1998, ApJ, 499, L5
76. Moore, B. 1994, Nature, 370, 629
77. Flores, R. A. & Primack, J. R. 1994, ApJ, 427, L1
78. McGaugh, S. S. & de Block W. J. G. 1998, 499, 41
79. Debattista, V. P. & Sellwood, J. A. 1998, ApJ, 493, L5
80. Moore, B., Quinn, T., Governato, F., Stadel, J. & Lake, G. 1999, MNRAS, 310, 1147
81. van den Bosch, F. C., Robertson, B. E., Dalcanton, J. J. & de Block, W. J. G. 2000, AJ, 119, 1579
82. Bolatto, A. D., Simon, J. D., Leroy, A. & Blitz, L. 2002, ApJ, 565, 238
83. Simon, J. D., Bolatto, A. D., Leroy, A. & Blitz, L. 2003, ApJ, 596, 957
84. Power, C., Navarro, J., Jenkins, A., Frenk, C. S., White, S. D. M., Springel, V., Stadel, J. & Quinn, T. 2003, MNRAS, 338, 14
85. Stoehr, F., White, S. D. M., Springel, V., Tormen, G. & Yoshida, N. 2003, MNRAS, 345, 1313
86. Navarro, J. F., Hayashi, E., Power, C., Jenkins, A. R., Frenk, C. S., White, S. D. M., Springel, V., Stadel, J. & Quinn, T. R. 2004, MNRAS, 349, 1039
87. Huss, A., Jain, B. & Steinmetz, M. 1999, ApJ, 517, 64
88. Rhee, G., Valenzuela, O., Klypin, A., Holtzman, J. & Moorthy, B. 2004, ApJ, in press, `http://arxiv.org` e–Print, astro–ph/0311020
89. Primack, J. 2004, in *Dark Matter in Galaxies*, proceedings of IAU Symposium 220, eds. S. D. Ryder, D. J. Pisano, M. A. Walker & K. C. Freeman (San Francisco:ASP) 53
90. Binney, J. & Tremaine, S. 1987, *Galactic Dynamics* (Princeton: Princeton University Press)
91. Hoeft, M. Mücket, J. P. & Gottlöber, S. 2004, ApJ, 602, 162
92. Bartelmann, M. 1996, A&A, 313, 697
93. Wright, C. O. & Brainerd, T. G., 2000, ApJ, 534, 34
94. Kauffmann, G., Colberg, J. M., Diaferio, A. & White, S. D. M. 1999, MNRAS, 303, 188
95. Madgwick, D. S., Lahav, O., Baldry, I. K., Baugh, C. M., Bland–Hawthorn, J., Bridges, T., Cannon, R., Cole, S., Colless, M., Collins, C. A., Couch, W. J., Dalton, G. B., De Propris, R., Driver, S. P., Efstathiou, G., Ellis, R. S., Frenk, C. S., Glazebrook, K., Jackson, C. A., Lewis, I. J., Lumsden, S., Maddox, S. J., Norberg, P., Peacock, J. A., Peterson, B. A., Sutherland, W. J. & Taylor, K. 2002, MNRAS, 333, 133
96. Conroy, C., Newman, J. A., Davis, M., Coil, A., Renbin, Y., Cooper, M. C., Gerke, B. F., Faber, S. M. & Koo, D. C. 2004, submitted to ApJ, `http://arxiv.org` e–Print, astro–ph/0409305
97. Davis, M., Gerke, B. F. & Newman, J. A. 2004, in *Observing Dark Energy: NOAO Workshop, March 18–20, 2004*, eds. S. Wolff & T. Lauer, `http://arxvig.org` e–Print, astro–ph/0408344
98. Zaritsky, D. & White, S. D. M. 1994, ApJ, 435, 599
99. Verheijen, M. A. W. 2001, ApJ, 563, 694
100. Sackett, P.D. 1999, in *Galaxy Dynamics*, ASP Conf. Series 182, eds. D. R. Merritt, M. Valluri & J. A. Sellwood, 393
101. Maller, A. H., Simard, L., Guhathakurta, P., Hjorth, J., Jaunsen, A. O., Flores, R. A., & Primack, J. R. 2000, ApJ, 533, 194
102. Keeton, C. R., Kochanek, C. S. & Falco, E. E. 1998, ApJ, 509, 561
103. Zibetti, S., White, S. D. M. & Binkmann, J. 2004, ApJ, 601, 556
104. Dubinski, J. & Carlberg, R. 1991, ApJ, 378, 496
105. Warren, M. S., Quinn, P. J., Salmon, J. K., & Zurek, W. H. 1992, ApJ, 399, 405
106. Blumenthal, G. R., Faber, S. M., Flores, R. & Primack, J. R. 1986, ApJ, 301, 27
107. Dubinski, J. 1994, ApJ, 431, 617
108. Kazantzidis, S., Kravtsov, A. V., Zentner, A. R., Allgood, B., Nagai, D. & Moore, B. 2004, ApJ, 611, L 2004
109. Natarajan, P. & Refregier, A. 2000, ApJ, 538, L113
110. Brainerd, T. G., & Wright, C. O. 2000, `http://arxiv.org` e–Print archive, astro–ph/0006281
111. Wright, C. O. & Brainerd, T. G. 2002, `http://arxiv.org` e–Print archive, astro–ph/0205297
112. Kochanek, C. S. 2002, in *The Shapes of Galaxies and their Halos*, ed. P. Natarajan (World Scientific), 62
113. Holmberg, E. 1969, Ark. Astron., 5, 305
114. Valtonen, M., Teerikorpi, P. & Argue, A. 1978, AJ, 83, 135
115. van den Bosch, F. C., Norberg P., Mo, H. J. & Yang, X. 2004 MNRAS, 352, 1302
116. Peñarrubia, J., Kroupa, P. & Boily, C. 2002, MNRAS, 333, 779
117. Abadi, M. G., Navarro, J. F., Steinmetz, M. & Eke, V. R. 2003, ApJ, 597, 21
118. Knebe, A., Gill, S. P. D., Gibson, B. K., Lewis, G. F., Ibata, R. A. & Dopita, M. A. 2004, ApJ, 603, 7
119. Moore, B., Ghigna, S., Governato, F., Lake, G., Quinn, T., Stael, J. & Tozzi, P. 1999, ApJ, 524, L19
120. Klypin, A., Kravtsov, A., Valenzuela, O. & Prada, F. 1999, ApJ, 522, 82